JOURNAL OF GEOPHYSICAL RESEARCH, VOL. 113, E08015, doi:10.1029/2007JE003017, 2008

The drying of Titan's dunes: Titan's methane hydrology and its impact on atmospheric circulation

Jonathan L. Mitchell[1]

Received 3 October 2007; revised 28 March 2008; accepted 16 April 2008; published 22 August 2008.

[1] We explore the effect of a finite reservoir of methane on Titan's atmospheric circulation, precipitation patterns, and surface methane content. We develop a soil model that accounts for the methane cycle in the surface-atmosphere system, and we implement this surface model in a two-dimensional model of the Titan's atmosphere. Seasonal oscillations in latitude of the large-scale circulation accomplish net drying of the low-latitude surface by diverging methane vapor from low latitudes to higher latitudes. Simulations with an initially deep methane reservoir indicate this mechanism is able to dry ~1.75 meters of liquid methane per Titan year from the low-latitude surface. The existence of low-latitude desert morphologies suggests that the system has had sufficient time to completely remove the surface methane by this mechanism. We then varied the reservoir size, focusing on initial depths of 30 meters of liquid methane or less and compared the results to available observations. The climate system has an abrupt transition to a warmer state with less precipitation and nearly global surface drying near the level at which the atmosphere can store the majority of the methane reservoir as vapor or around 6.5 meters of equivalent liquid methane for our particular choice of parameters. A comparison of our model results with Huygens' observations suggests Titan's climate mimics a state in which most of the methane inventory with direct access to the atmosphere (i.e., excluding underground sources) is stored in the atmosphere.

Citation: Mitchell, J. L. (2008), The drying of Titan's dunes: Titan's methane hydrology and its impact on atmospheric circulation, *J. Geophys. Res.*, *113*, E08015, doi:10.1029/2007JE003017.

1. Introduction

[2] Though speculation of a global methane ocean on Titan was once pervasive, Cassini and ground-based observations have shown Titan's landscape is devoid of large oceans [*West et al.*, 2005; *Porco et al.*, 2005]. Indeed, much of the surface is arid, with dunes covering a significant fraction of the landscape [*Lorenz et al.*, 2006], while methane lakes appear to be confined primarily to northern high latitudes [*Stofan et al.*, 2007]. Fluvial erosion features are prevalent [*Stofan et al.*, 2006], most likely indicating methane rain occurs or has occurred over a large area of the surface. Huygens measurements suggest at least some of the low-latitude surface could be wetted with liquid methane, though a solid "crust" may isolate the methane from the atmosphere [*Zarnecki et al.*, 2005].

[3] To date, convective methane clouds have only been observed at mid and high southern latitudes, where the season is progressing from summer to fall [*Roe et al.*, 2002, 2005a; *Griffith et al.*, 2005; *Schaller et al.*, 2006; *Hirtzig et al.*, 2006, 2007]. Cloud-resolving models predict these storms could produce tens of kg/m^2 of precipitation in a few hours [*Hueso and Sànchez-Lavega*, 2006; *Barth and Toon*, 2006; *Barth and Rafkin*, 2007]. Methane vapor is subsaturated at low latitudes [*Niemann et al.*, 2005], and some lifting mechanism would be needed to trigger cloud formation there [*Barth and Toon*, 2006; *Barth and Rafkin*, 2007], while methane concentrations at mid and high latitudes remain unconstrained. Huygens observed a methane "haze" layer near 21 km altitude, which has been interpreted as a stratiform cloud producing 55 mm/yr of precipitation [*Tokano et al.*, 2006b]. Turbulent motions observed between 20 and 30 km altitude give further evidence for the existence of a stratiform cloud [*Lorenz et al.*, 2007].

[4] Atmospheric models of Titan indicate observed clouds owe their existence to dynamical transports by the atmosphere. Simulations by *Rannou et al.* [2006] reproduce observed clouds by slantwise meridional overturning cells transporting moisture from low to mid and high latitudes. Large seasonal oscillations of the Hadley circulation in simulations by *Mitchell et al.* [2006] suggest the observed clouds mark large-scale updrafts of the general circulation, and isolated clouds can only be produced with the effects of methane thermodynamics included.

[5] *Mitchell et al.* [2006] also showed the thermal inertia, as measured by the phase lag of the large-scale updraft with the solar forcing, is sensitive to the supply of methane from the surface. They attributed this sensitivity to the stiffening of the system against the time-dependent seasonal forcing

[1]Department of Astronomy and Astrophysics, University of Chicago, Chicago, Illinois, USA.

0148-0227/08/2007JE003017$09.00

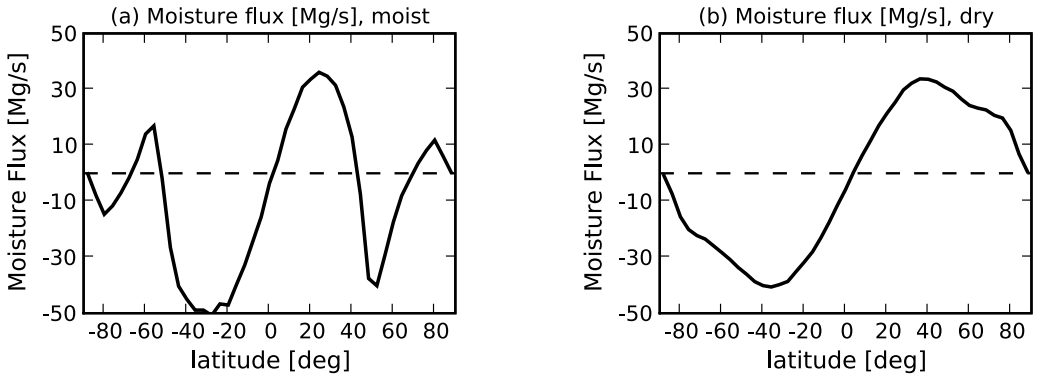

Figure 1. Annual and vertical mean moisture fluxes (Mg/s, positive northward) in two simulations from *Mitchell et al.* [2006].

by the latent energy flux from methane evaporated into the atmosphere from the surface. The surface, which is mostly solid, has low heat capacity relative to the atmosphere, which has considerable mass and weak radiative fluxes. In the absence of destabilizing effects of methane vapor, instantaneous surface warming by sunlight triggers dry convection which warms only a shallow layer of the atmosphere. Methane evaporated into the lowest layers produces deep convection so that more mass of the high-heat-capacity atmosphere is warmed; the resulting circulation has greater thermal inertia as measured by the phase lag with solar forcing.

[6] All previous atmospheric models of Titan incorporating the effects of methane thermodynamics have assumed liquid methane exists in infinite supply at the surface [*Tokano et al.*, 2001; *Rannou et al.*, 2006; *Mitchell et al.*, 2006]; we refer to this type of model as "aquaplanet" simulations. These simulations show the atmosphere diverges methane out of the low latitudes. This divergence is balanced by annual mean drying of the low-latitude surface; however, since methane was assumed to exist in infinite supply, the surface never dries out. The lack of standing liquids over much of the surface [e.g., *Stofan et al.*, 2006; *Lorenz et al.*, 2006] and sensitivity of models to the surface supply of methane [*Mitchell et al.*, 2006] suggest a full accounting of the cycle of a finite methane reservoir is needed to characterize the climatology of Titan's methane cycle.

[7] Here we present axisymmetric simulations of Titan's atmosphere that account for a limited supply of methane by replacing the surface model of *Mitchell et al.* [2006] with a soil model similar to those used in Earth general circulation models (GCMs) [*Robock et al.*, 1995]; we refer to this version of our model as a "terraplanet". The terraplanet model is the opposite limit to the previous assumption of infinite surface supply of methane, and represents the first step toward characterizing the effect of a limited methane reservoir size and solid surface on observed phenomena. We begin by motivating the development of the terraplanet model in section 2. We describe the model in section 3. In section 4, we demonstrate the surface-drying rate of the climate system. We discuss simulations with a range of total methane reservoirs in section 5, compare representative examples to observations in section 6, and then offer possible interpretations in section 7. In section 8 we conclude and outline future directions.

2. Motivation: Surface Drying in Aquaplanet Simulations

[8] In "aquaplanet" simulations of Titan, the atmosphere diverges methane out of low latitudes resulting in net drying of the low-latitude surface [*Rannou et al.*, 2006; *Mitchell et al.*, 2006]. The *Mitchell et al.* [2006] simulations produce a meridional overturning circulation, or Hadley cell, that is global in extent. Near equinoxes there are two equatorially symmetric Hadley cells with a common updraft near the equator and downdrafts near the poles. At solstices, a single cross-equatorial Hadley cell dominates. The large-scale updraft of the Hadley cell(s) with associated surface-level convergence of air is referred to as the Inter-Tropical Convergence Zone (ITCZ); the lifting of air in the ITCZ tends to condense out methane due to the adiabatic cooling of air parcels as they rise in altitude. Methane evaporated into the surface-level air of the Hadley cell is converged to the ITCZ where it is precipitated out. Because of the global extent of the Hadley circulation, almost all precipitation occurs in the ITCZ and all other latitudes experience surface drying. Instantaneous surface drying in itself doesn't guarantee net (seasonally averaged) surface drying at any particular latitude since the precipitating ITCZ oscillates from deep in one hemisphere to the other with season [see *Mitchell et al.*, 2006]. However, the strongest overturning and greatest amount of precipitation occurs during solstices when the ITCZ is located off equator. Therefore large areas of the low-latitude surface experience net drying due to divergence of methane vapor by the atmosphere in these latitudes. The same mechanism is responsible for creating and sustaining deserts on Earth on the poleward flanks of the tropics; steady sea surface temperatures keep the ITCZ near the equator so the areas of net surface drying are always located poleward of the ITCZ. The mechanism for drying the low-latitude surface by a seasonally oscillating ITCZ is a robust feature in climates with atmospheres containing a condensible substance and a solid surface; *Pierrehumbert* [2005] saw similar low-latitude divergence of moisture in simulations of a hard snowball Earth climate.

[9] Figures 1a and 1b show the annual and vertical mean moisture flux in Mg/s (defined positive northward) in the

Table 1. Model Components and Parameters Differing Between This Study and the Simulations Performed by *Mitchell et al.* [2006]

Parameter	This Study	*Mitchell et al.* [2006]
Surface moisture model	soil	infinite reservoir
Infrared optical depth	9	3.33
Albedo, %	55	0
Stratospheric sw absorption, %	15	0
Tropospheric sw absorption, %	20	0
Boundary layer depth, mbar	1000	1275
Boundary layer diffusion, m^2/s	0.01	1

two simulations from *Mitchell et al.* [2006]. The divergence of the moisture flux is balanced by either surface drying or accumulation of liquids; positive(negative) slope in the moisture flux corresponds to drying(moistening) of the surface. The simulations differ in the amount of methane vapor that is evaporated from the surface into the atmosphere and the humidity threshold for convection to occur in the atmospheric interior. The ''moist'' case has unrestricted methane evaporation from the surface [see *Mitchell et al.*, 2006] for a more thorough description). The ITCZ oscillates between mid latitudes in one hemisphere to the other; the range of this oscillation roughly marks the area of methane vapor divergence (positive slope) in the low latitudes in Figure 1a. In the ''intermediate'' case, Figure 1b, surface methane evaporation is restricted, and the amplitude of latitudinal oscillations of the ITCZ is larger than in the ''moist'' case, which results in a wider range of latitudes from which methane vapor is diverged. However, since methane was assumed to exist in infinite supply, the surface never dries out. These simulations, with infinite surface methane supply, suggest a feedback may exist between the extent of surface drying and the amplitude of latitudinal oscillations of the large-scale circulation, which serves as the primary motivation for this study. The full extent of this feedback requires an accounting of a fixed methane reservoir, which we will carry out in the following sections.

3. Model Description

[10] Our terraplanet model builds on the atmospheric components used by *Mitchell et al.* [2006] including a zonally symmetric atmosphere, a boundary layer scheme with fixed diffusion coefficient and layer depth, a moist convection scheme [*Frierson*, 2007], large-scale condensation, and gray infrared radiation. In order to explore a wide range of initial conditions in a reasonable amount of computational time, we run the model at roughly half the resolution used by *Mitchell et al.* [2006]: 14 vertical levels with midpoints spaced evenly in pressure from 1450–50 mbar (~0.7–70 km) and 21 gridpoints in the horizontal. We find this reduction in resolution does not significantly change the simulations in *Mitchell et al.* [2006]. A more detailed description of the model follows, and additional modifications to model parameters are summarized in Table 1.

3.1. Dynamical Core

[11] We employ the zonally symmetric primitive equations to model atmospheric circulations [*James*, 1994]. We discretize the two-dimensional model equations by finite difference on a grid spaced evenly on 14 pressure levels and 21 latitudes. Equally spaced pressure levels imply equal mass per layer and therefore devote most of the resolution to the lower atmosphere; we use this approach since we are interested in the lower layers where the cycle of methane evaporation and precipitation is occurring. The zonally symmetric equations conserve angular momentum in the free troposphere where friction effects are negligible [*Held and Hou*, 1980], and therefore do not allow the development of superrotation. The simplifying assumptions in our dynamical core are motivated by the hypothesis that the zonal mean flow determines the climatology of the tropospheric methane cycle. We will evaluate the legitimacy of our assumption of zonal symmetry by comparing the extent to which our simulations agree or disagree with observations of circulations in the lower atmosphere in section 6.

3.2. Soil Model

[12] For terraplanet simulations, we introduce a simplified soil model that replaces the infinite liquid surface reservoir used by *Mitchell et al.* [2006]. The soil model consists of a surface that is covered by a grid of ''buckets'' equally spaced along the meridian; this layout implies the number of buckets per latitude circle grows with the cosine of the latitude. The liquid methane at the surface is allowed to evaporate, be redistributed by large-scale winds, and precipitate back to the surface. The soil model keeps account of the net accumulation at the surface, and when individual surface elements dry out, the evaporative flux is locally shut off. Each bucket has an infinite capacity to store liquid methane, so any net accumulation does not run off into adjacent buckets but deepens the local reservoir. We restrict the total methane reservoir to be finite and allow the methane to be redistributed in the surface-atmosphere system. This approach is intended to model the methane reservoir that is currently in direct contact with the atmosphere; we make no attempt to account for a potential subsurface reservoir that may exist isolated from the atmosphere on seasonal timescales.

[13] The prognostic equation for surface temperature with energy fluxes defined positive downward is

$$C\,\frac{\partial T_s}{\partial t} = F_{lat} + F_{sen} + F_{IR} + S - \sigma T_s^4, \qquad (1)$$

where C is the heat capacity of the surface, F_{lat} is the latent heat flux, F_{sen} is the sensible (dry) heat flux, F_{IR} is the infrared back radiation from the atmosphere, S is the fraction of insolation reaching the surface, σ is the Stefan-Boltzmann constant, and T_s is the surface temperature. The surface is assumed to be a single slab of uniform, specified heat capacity per unit area of ~200,000 $J/m^2/K$, which is near the value assigned to a ''porous icy regolith'' in *Tokano* [2005]. (This heat capacity corresponds to a timescale of 10 Earth days for a surface radiating at 95 K.) While this heat capacity is low for putative hydrocarbon lakes [*Tokano*, 2005], the heat capacity of the atmosphere is at least an order of magnitude larger, so for the sake of simplicity we keep the surface heat capacity fixed regardless of the surface

conditions (i.e., the presence or absence of liquid methane). The turbulent fluxes are diagnosed in the model as

$$F_{lat} = \begin{cases} -C_d \rho U L_v (q_s - q_0) & \text{for } W_{soil} > 0, \rho_s < \rho_0 \\ -C_d \rho U L_v (q_s - q_0) e^{-\frac{(\rho_s - \rho_0)}{\rho_e}} & \text{for } W_{soil} > 0, \rho_s > \rho_0 \\ 0 & \text{otherwise,} \end{cases} \quad (2)$$

and

$$F_{sen} = \begin{cases} -C_d \rho U C_p (T_s - T_0) & \text{for } \rho_s \\ -C_d \rho U C_p (T_s - T_0) e^{-\frac{(\rho_s - \rho_0)}{\rho_e}} & \text{for } \rho_s > \rho_0, \end{cases} \quad (3)$$

where W_{soil} is the soil moisture depth, C_d is a bulk exchange coefficient, U is a parameter representing the surface wind, L_v is the latent heat of vaporization, q_s is the saturation mass mixing ratio of methane at the surface temperature, q_0 is the mass mixing ratio of methane at the temperature of surface-level air (~700 m), ρ_s is the density of saturated air at the surface temperature, ρ_0 is the density of surface-level air, ρ_e is a specified e-folding parameter, C_p is the specific heat of nitrogen, T_s is the surface temperature, and T_0 is the temperature of the surface-level air (~700 m). As can be seen in equation (2), the evaporative flux is shut off as the surface dries. The saturation mass mixing ratio of methane is modeled in a simplified manner by the Clausius-Clapeyron equation

$$q_s(T) = q_0 e^{(L_v/R_v)(1/T_0 - 1/T)}, \quad (4)$$

where R_v is the gas constant for methane and q_0 and T_0 are the triple point mass mixing ratio and temperature of methane, respectively.

[14] We use a value of C_d typical of Earth, 1×10^{-3}. U is a fixed parameter, and is given the value 5 m/s. The turbulent fluxes can be made to be dependent on magnitude of the surface-level wind, $|u|$. By holding U constant, we are removing the dynamic feedback between surface-level winds and turbulent fluxes. The actual surface wind can exceed that produced in models, and for this reason U can be thought of as a "gustiness parameter". We have not explored the sensitivity of our results to this assumption, and we plan to do so in future work.

[15] The exponential factor in equations (2) and (3) accounts for the attenuation of turbulent fluxes in the presence of an inversion, when the density of surface-level air, ρ_s, is heavier than the air above it, ρ_0. (To lowest order, the inversion is the result of surface temperatures being lower than the atmospheric temperature in contact with the surface, but the presence of methane also contributes to buoyancy.) Such inversions are common in the simulations in areas of strong evaporation. If this attenuation is not included, the linear formulae predict large atmosphere-to-surface sensible heat fluxes balance large surface-to-atmosphere latent fluxes; this scenario is unphysical since turbulence cannot operate efficiently in a stable boundary layer [*Garratt*, 1992]. We give ρ_e the value 0.01 kg/m^3 which generally prevents turbulent fluxes from exceeding the top-of-atmosphere insolation.

[16] The prognostic equation for the soil moisture depth, W_{soil}, is

$$\frac{\partial W_{soil}}{\partial t} = P - E \quad (5)$$

where P is the precipitation which results from convection and large-scale condensation,

$$E = -\frac{F_{lat}}{L_v \rho_v} \quad (6)$$

is the surface evaporation, and ρ_v is the density of liquid methane.

[17] Part of our goal is to assess the hypothesis that the unsaturated air measured by the Huygens probe at low latitudes [*Niemann et al.*, 2005] arises due to the redistribution by the atmosphere of a limited, geographically isolated surface reservoir of liquids. *Mitri et al.* [2007] have performed a simplified calculation of this sort using predicted advection timescales from a GCM (taken from *Tokano et al.* [2001]). They conclude methane lakes covering a very small fraction of the surface can produce intermediate near-surface humidities observed at low latitudes, but a few steps of the calculation merit discussion. First, *Mitri et al.* [2007] overestimate the evaporative flux by allowing an unphysically large, compensating sensible energy flux. As discussed in the preceding paragraph, surface fluxes predicted by the purely linear bulk aerodynamic formulae are valid only when the boundary layer is unstable, which is not realized over evaporating hydrocarbon lakes where the surface is cooler than the overlying air. Second, they assume that all methane is locally precipitated as the advection/overturning timescale approaches zero. However, condensation requires lifting by convergence which does not follow from a short advection timescale, and in fact the argument goes in the opposite direction. For thermodynamic reasons, the mass flux of the overturning circulation increases in the absence of latent heat release (condensation), while the depth of the overturning cell decreases. (The strength of a Hadley circulation is set by the heat transport required to keep temperatures horizontally uniform (the angular momentum constraint). In the absence of latent heat release by condensation, the atmosphere tends toward a statically stable state; the mass flux of the Hadley cell must increase dramatically in order to do enough work against the nearly neutral state to transport heat (see *Held and Hou* [1980] and *Caballero et al.* [2008]). Both of these effects decrease the overturning timescale, and it is in this "dry" state that methane vapor would be well mixed by the circulation.

[18] *Mitri et al.* [2007] also include depression of methane vapor pressure by dissolved nitrogen and ethane. As *Mitchell et al.* [2006] have shown, depression of the methane vapor pressure does have a feedback on the atmospheric circulation in simulations with a global surface reservoir of methane. In our present model, however, we do

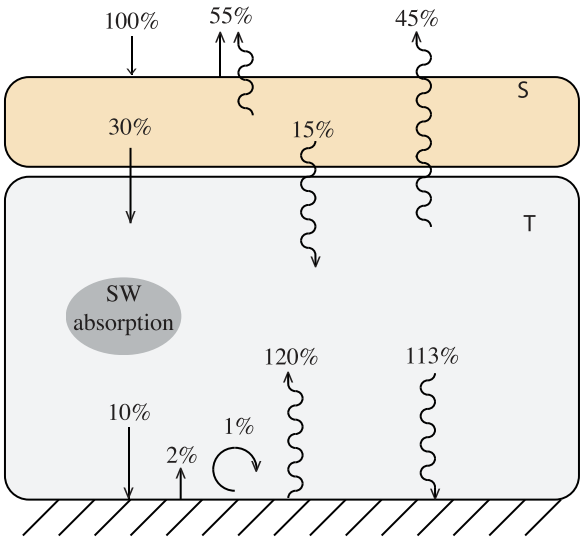

Figure 2. Schematic of the energy balance for a one-dimensional global-average radiative-convective model of Titan. Energy fluxes are normalized to the top-of-atmosphere solar radiation. Straight lines indicate shortwave fluxes, wavy lines indicate infrared fluxes, the circle indicates convective fluxes, the gray box is the troposphere, and the orange box is the stratosphere. Fluxes represent those produced in the model of *McKay et al.* [1991].

not take into account a lowering of the methane vapor pressure in order to cleanly isolate the effect on methane humidity of mechanical mixing of dry and moist air by the large-scale circulation.

3.3. Betts-Miller Moist Convection Scheme

[19] The Betts-Miller scheme relaxes temperature to a moist adiabat, and moisture to specified relative humidity with respect to the moist adiabat, which is calculated using the simplified Clausius-Clapeyron relation, equation (4). A correction is additionally applied to the temperature relaxation to ensure conservation of energy. Shallow (nonprecipitating) convection occurs when precipitation is predicted to be less than zero, that is, when convection is favorable but it does not produce condensation. The only parameters of the scheme are the convective relaxation time and the reference profile relative humidity. *Frierson* [2007] shows that the general circulation in a model with gray radiative transfer is quite insensitive to each of these parameters, provided significant large-scale condensation does not occur. Use of the simplified Betts-Miller scheme additionally improves the resolution sensitivity of the tropical general circulation. For general circulation models of the Earth, the use of convection schemes is necessary to obtain a proper strength Hadley circulation and realistic precipitation distribution. The simplified Betts-Miller scheme is a unique convection scheme in that its parameters are not tuned to Earth-like conditions, and can be used for any planetary atmosphere.

[20] While we do not explicitly account for the lowering of the partial pressure of methane due to dissolved nitrogen [*Thompson et al.*, 1992], the ~20% effect is implicitly taken into account through the relative humidity parameter, which we set to 80%. We also do not account for the ~10% lowering of the latent heat of condensation.

3.4. Radiation Model

[21] We use a gray, infrared radiative transfer scheme [*Mitchell et al.*, 2006] augmented with parameterized shortwave absorption. The gray model neglects the radiative feedback of methane, which has been shown to be important for determining stability in one-dimensional climate models [*Lorenz et al.*, 1999]. Effects of the stratospheric haze are imposed as an upper boundary condition and shortwave absorption in the lower atmosphere is assumed to attenuate the solar beam linearly with pressure. We use parameters that reproduce radiative fluxes at the upper and lower boundaries of the troposphere of a full radiative transfer model of *McKay et al.* [1989], which is represented schematically in Figure 2. 55% of the solar radiation is reflected directly back to space to account for shortwave scattering and infrared radiation escaping directly from the stratosphere to space, 15% of the incoming solar radiation is reprocessed into downwelling infrared radiation at the top of the atmosphere, and 20% of the remaining solar radiation is absorbed in the troposphere, leaving only 10% of the solar radiation to be absorbed by the surface (see Figure 2). We increase the infrared optical depth relative to the value used in *Mitchell et al.* [2006] to $\tau_\infty = 9$ to offset the cooling of the surface by shortwave absorption and thereby constrain radiative equilibrium surface temperatures to be close to the observed near-equatorial value [*Fulchignoni et al.*, 2005]. The infrared back radiation from the atmosphere then matches that produced in the full radiation scheme, ~113% of the incoming solar radiation. The surface cools at a blackbody temperature of 94K, which is 120% of the incoming solar radiation. We impose pressure broadening roughly in accordance with the Rosseland mean opacity determined from a full radiative transfer code, $\tau \propto p^{1.5}$ [*McKay et al.*, 1991]. The gray approximation does not account for the infrared "window" in the absorption spectrum at 500 cm^{-1} [*McKay et al.*, 1989]. The dashed line in Figure 11a shows the radiative equilibrium temperature profile of our model and the Huygens temperature profile is shown as the solid red line [*Fulchignoni et al.*, 2005]. There is generally good agreement between our model and the observed profile below 200 mbar; errors in the temperature profile of the stratosphere are tolerable because the stratosphere has such little mass.

3.5. Boundary Layer Parameters

[22] Subgridscale turbulence in the planetary boundary layer is modeled by a diffusion over a fixed layer depth, and takes the form

$$\left(\frac{\partial}{\partial t}\right)_{diff} = \frac{\partial}{\partial p}\left(\nu g^2 \rho^2 \frac{\partial}{\partial p}\right), \qquad (7)$$

where p is pressure, ν is a diffusion coefficient, g is the surface gravity, and ρ is the atmospheric density. We fixed the boundary layer depth to 1000 mbar (roughly 8 km altitude) since observations of the vertical profile of methane concentration suggest Titan has a well-mixed boundary layer of this depth [*Niemann et al.*, 2005]. Because of the reduced solar forcing at the surface in our

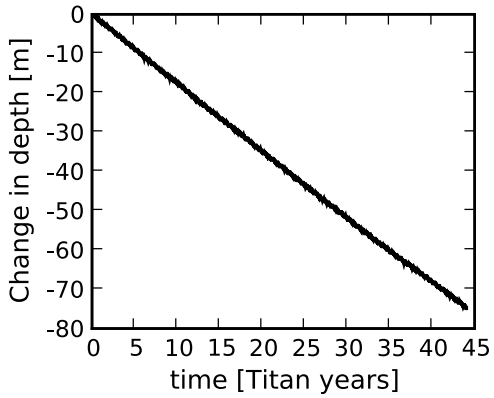

Figure 3. The average change in soil moisture depth in meters between 20N/S versus time for the initially deep reservoir case.

radiation scheme, our simulated solstitial polar surface temperatures are attenuated relative to the simulations in *Mitchell et al.* [2006], which inhibits the development of solstitial polar precipitation features. However, we found that lowering the magnitude of boundary layer diffusion allows the formation of precipitation at the solstitial pole. There is observational support for lowering the boundary layer diffusion. *Tokano et al.* [2006a] used Huygens temperature and pressure observations to constrain properties of the turbulent boundary layer; their results suggest a lower value of diffusion coefficient than what was used by *Mitchell et al.* [2006] is more appropriate, and the current simulations take this lower value, $\nu_v = 0.01$ m^2/s. For this value of diffusion, the Ekman number, $E = \nu_v/(2\Omega d^2)$ where Ω is the planetary rotation rate and d is the characteristic depth of turbulent eddies in the boundary layer, drops to 0.1 at a depth of 150 m, which is a factor of 2 smaller than the 300 m suggested by *Tokano et al.* [2006a]. At 1000 mbar (8 km), the Ekman number drops to $E = 3 \times 10^{-5}$, so our choice of the depth of the boundary layer is somewhat irrelevant. We discuss further implications of this change on our model simulations in Appendix A.

4. Model Surface Drying Rate

[23] Our approach is to initialize model runs with a finite, uniform soil moisture depth and a dry atmosphere and allow the climate system to self-consistently redistribute the available moisture until a statistical steady state is reached.

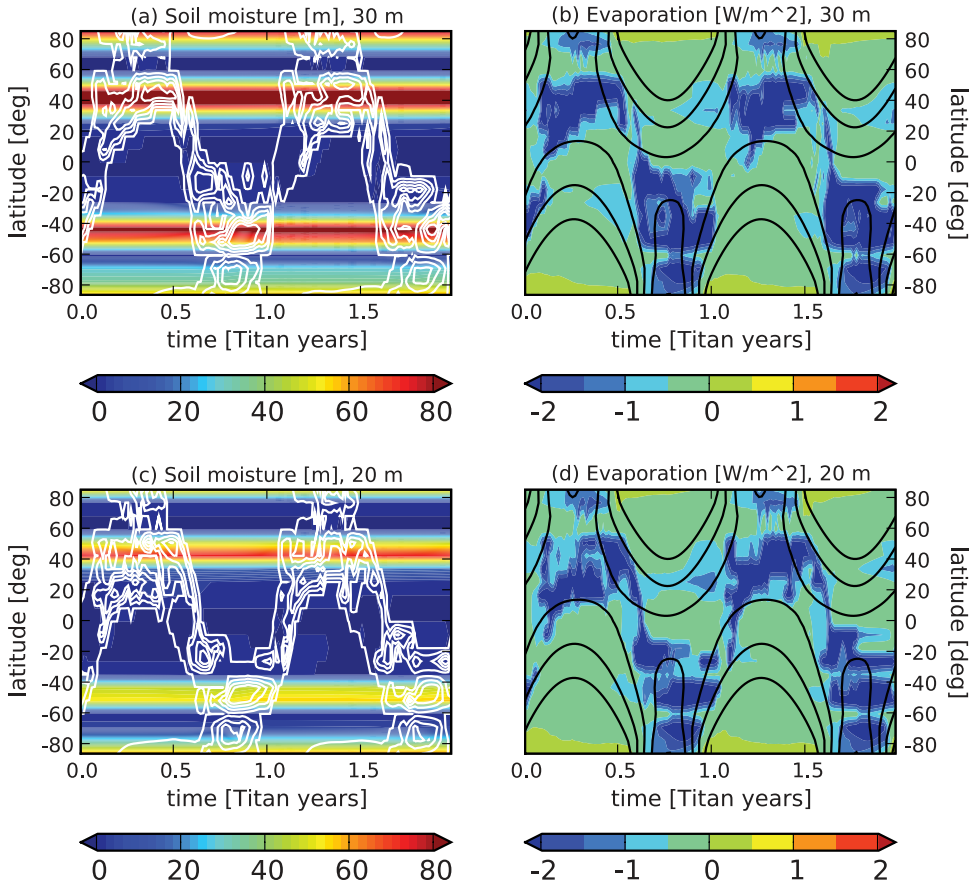

Figure 4. (a and c) Soil moisture depth in meters (solid contours) and precipitation (open contours) for the last two model years beginning at Northern Spring Equinox in our simulations. Precipitation contours are spaced at 0.5 mm/day intervals from 0 to 2 mm/day in all cases. (b and d) Evaporative flux in W/m^2 with negative values indicating evaporation from the surface (solid contours) and insolation pattern (solid contours) for the same time interval.

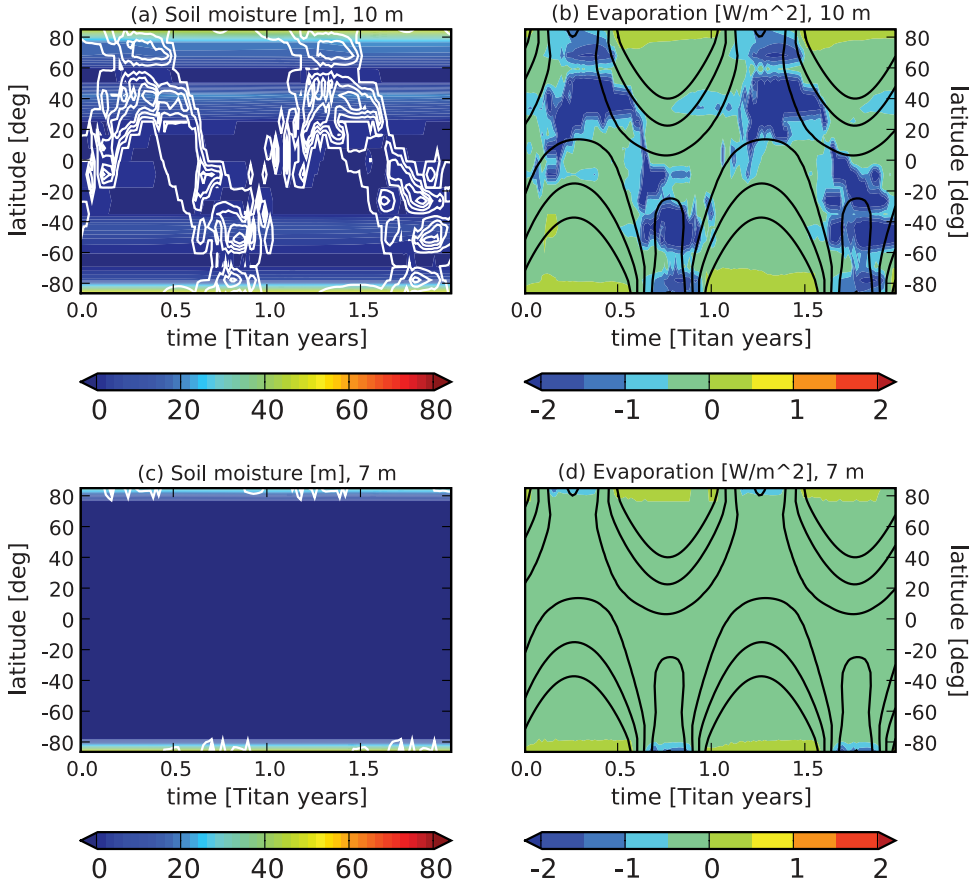

Figure 5. Same as in Figure 4 for 10-m and 7-m initial methane reservoir depths.

Our first step is to determine the rate at which the surface-atmosphere system redistributes surface methane. To accomplish this, we initialize the surface reservoir with a very large amount of liquid methane (10^6 m). Based on simulations by *Rannou et al.* [2006] and *Mitchell et al.* [2006], we expect the low latitudes to dry considerably due to large-scale atmospheric transport of methane, while mid and high latitudes could see considerable buildup of the local methane reservoir due to precipitation.

[24] Figure 3 shows the change in soil moisture depth averaged between 20N/S as a function of time for the initially deep reservoir case. The change in soil moisture, equation (5), balances methane vapor divergence in the atmosphere. The figure shows the rate of change for our model is constant with time at ~1.75 meters of liquid methane per Titan year. The existence of low-latitude dunes [*Lorenz et al.*, 2006] suggests this mechanism has operated long enough for the low-latitude surface to dry out. In order to establish a lower limit on the size of the methane inventory with access to the atmosphere, additional information on the time during which the inventory has been constant or decreasing and the timescale for surface/subsurface flow of methane is required.

[25] Since the vast majority of Titan's surface is devoid of oceans [*Stofan et al.*, 2006], a very deep reservoir with access to the atmosphere can be ruled out. We somewhat arbitrarily choose to run our simulations for 50 Titan years, so we expect our model to produce completely dry surface conditions at low latitudes for initial reservoirs at or below ~90 meters. In the following section, we discuss the sensitivity of our model to initial methane reservoirs below this level.

5. Model Sensitivity to Initial Methane Reservoir Size

[26] We performed a series of simulations over a range of initial methane reservoir depths from 30 to 7 m of methane. Figures 4 and 5 show the soil moisture depth in meters (solid contours) and precipitation patterns (open contours) in the left column and surface latent flux in W/m^2 (solid contours) and insolation pattern (solid contours) in the right column over the last two Titan seasons of our simulations for this range of initial reservoirs. In time-series plots, the seasons correspond to the following: time = 0, 1, 2 – northern spring equinox; time = 0.28, 1.28 – northern summer solstice; time = 0.5, 1.5 – southern spring equinox; and time = 0.77, 1.77 – southern summer solstice. The "Huygens epoch", i.e., the season at which the Huygens probe landed on Titan, roughly corresponds to time = 0.84, 1.84. The low-latitude dried region spans from 30N to 30S in most cases; there is very little change in the width of the low-latitude dried region for initial reservoirs deeper than 10 m. Note that the low latitudes do receive precipitation at some seasons, but the precipitation does not accumulate over a given year. In the 30 m and 20 m cases, the ITCZ deposits a large amount of methane at mid latitudes; as in the moist limit by *Mitchell et al.* [2006], the availability of

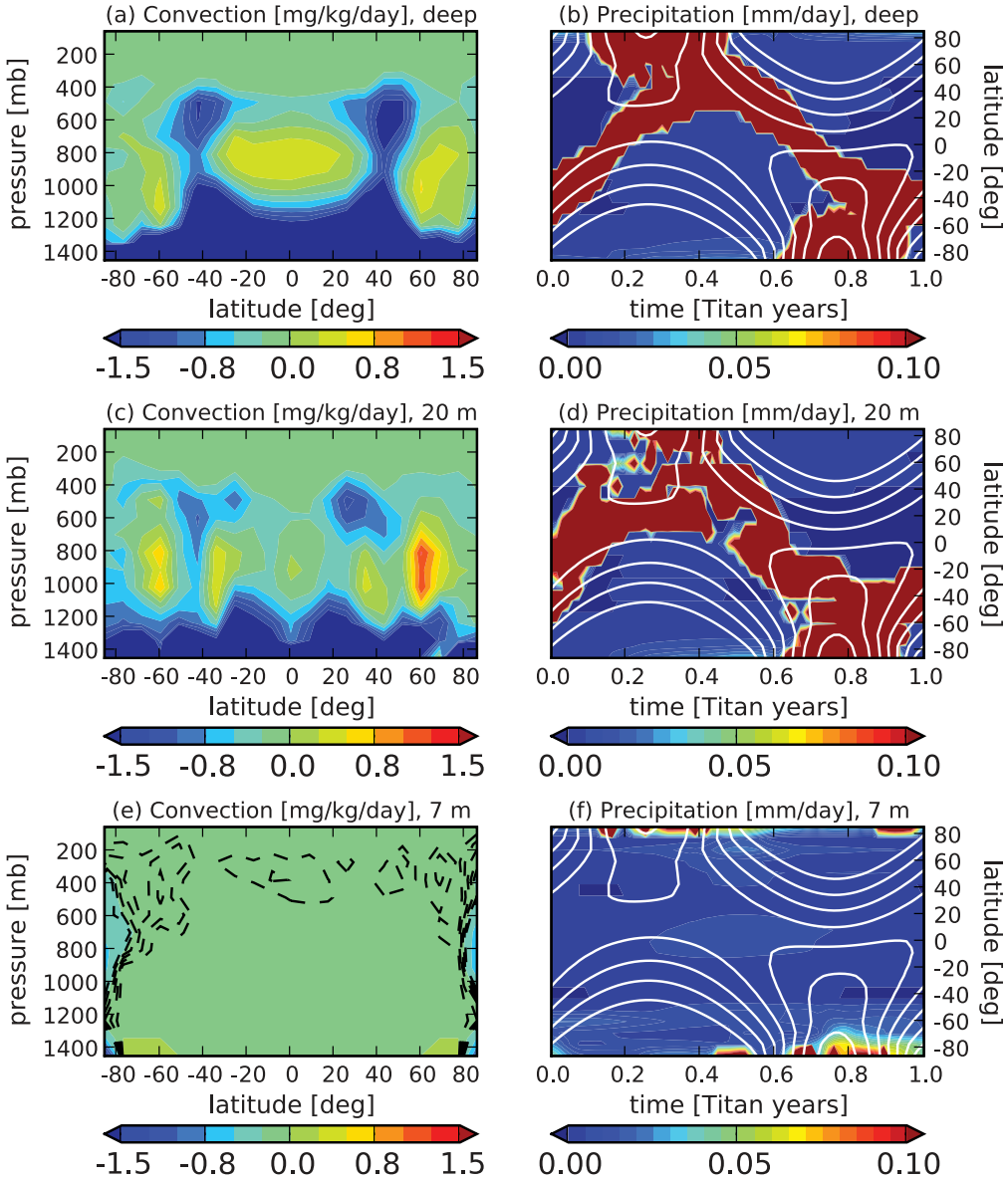

Figure 6. Plots of convective tendencies and precipitation for three initial methane reservoir sizes. (left column) Annual-mean moistening (negative values imply drying/condensation) in mg/kg/day. The dashed lines in the 7-m case are the convective moistening rate spaced at intervals of 0.5 mg/kg/day from −0.3 to 0. (right column) 10-Titan-day average precipitation in mm/day (solid contours) and insolation pattern (lines).

surface methane at mid and high latitudes produces deep convection which warms a deeper portion of the high-thermal-inertia atmosphere and halts the poleward progression of the ITCZ near solstices. As a result, the soil moisture accumulates at midlatitudes. Evaporation, which by convention is negative when directed from the surface to the atmosphere, primarily occurs locally in the areas of the most intense precipitation. Some "dewing" occurs at the winter poles, which is evident as positive (downward directed) evaporation. As the initial reservoir is reduced, precipitation in the ITCZ becomes more variable, the depth of the midlatitude surface moisture shallows, the ITCZ penetrates to slightly higher latitudes, and the horizontal extent of the low-latitude dry region widens. Precipitation also becomes more sparse in the 10 m reservoir case, and the surface is becoming very dry everywhere except at the very highest latitudes. At 7-m reservoir depth, the climate system has crossed into a different regime; the ITCZ can no longer maintain midlatitude soil moisture, and the ITCZ is free to move from pole to pole as in the dry limit by *Mitchell et al.* [2006]. Precipitation in the 7 m reservoir case tends to occur in brief, torrential downpours; the magnitude of these downpours is a few times larger than the maximum precipitation in the other three cases.

[27] In subsequent analysis, we narrow our focus further to three representative cases: the deep reservoir limit, the 20-m reservoir, and the 7-m reservoir.

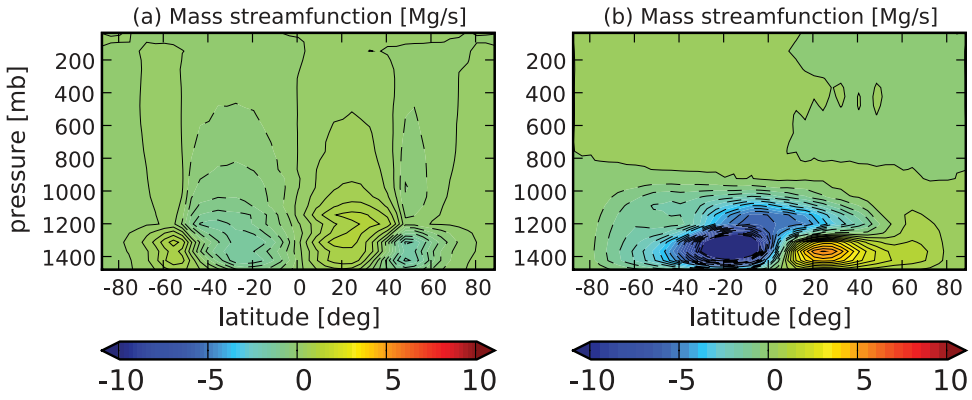

Figure 7. Annual-mean mass fluxes [Mg/s] in moist and dry simulations from *Mitchell et al.* [2006]. Positive (negative) fluxes indicate counterclockwise (clockwise) circulation.

5.1. Convection and Precipitation

[28] Figure 6 shows the annual-mean moistening in the free troposphere in the left column and instantaneous precipitation (solid contours) in the right column for our three representative cases. We have intentionally chosen a color scale that enhances weak precipitation features; red regions correspond to areas receiving more than 0.1 mm/day of precipitation. Since our model atmosphere does not have a cloud model, we use moistening (negative values correspond to drying) as a proxy for cloud formation. The convection scheme is intended to model the unresolved motions and physics in our model. Convection produces strong updrafts which dries the surface-level air and produces precipitation aloft. In some cases, convection dries (negative moistening) the entire column, and in others it dries surface-level air and air near the tropopause while moistening intermediate layers. In the 7 m case, the convection scheme is only triggered at the summer solstitial poles. Precipitation at lower latitudes (equatorward of 80N/S) is primarily the result of large-scale precipitation (condensation when a gridbox becomes saturated) which can moisten lower layers by re-evaporation.

[29] Deep convection associated with the large-scale updraft is clearly dominating the precipitation in the deep and 20 m reservoir cases. The strongest annual-mean drying in Figures 6a and 6c is seen at mid latitudes between the ground and 600 mbar. Condensation halts at around 400 mbar, corresponding to roughly 30 km altitude which is within the range of cloud heights, 20–40 km, observed by Cassini [*Griffith et al.*, 2005]. There is very weak precipitation evident at the winter poles in Figures 6b and 6d, which results from grid-scale condensation due to dropping temperatures. (Cassini has observed a large cloud capping the winter pole [*Griffith et al.*, 2006]. Though the cloud is thought to be ethane, it could also be the condensation of methane seen in our model). Other precipitation patterns in the 20 m and deep cases are similar to the moist simulations discussed in *Mitchell et al.* [2006], including a meandering ITCZ that is out of phase with the seasonal forcing and solstitial polar and high-latitude precipitation in phase with the seasonal forcing. The annual mean precipitation rate is ~0.5 cm per Earth year, in good agreement with previous estimates of the available evaporative flux [*Lorenz*, 2000]; the instantaneous precipitation rate locally exceeds this value due to large-scale convergence of latent energy by the atmosphere. The dry low-latitude surface in the 20-m case introduces more variability in the ITCZ; precipitation due to the ITCZ has discontinuities in the time series in the 20-m case, particularly when entering the dried region from moist surface regions at higher latitudes. The precipitation patterns at mid and high summer latitudes in both cases are consistent with the available cloud observations.

[30] The 7-m reservoir case displayed in Figures 6e and 6f shows very different precipitation and cloud patterns. The strongest convective drying is isolated to high latitudes in the annual-mean, which correspond to the isolated precipitation bursts seen at high summer latitudes in Figure 6f. Our model output is averaged over 10 Titan days (160 Earth days), and so brief, intense storms can be severely diluted by averaging. The most intense events produce ~3.5 mm/day precipitation rates; over the 160 day period this corresponds to 250 kg/m^2. One might imagine several storms with lifetimes of ~8 hours occurring in the span of 10 Titan days, in which case each individual storm would need to produce 50–100 kg/m^2, which is similar in magnitude to predictions of intense convection in cloud-resolving models [*Hueso and Sànchez-Lavega*, 2006; *Barth and Rafkin*, 2007]. The widespread, weaker drying seen at all latitudes near the tropopause in the annual mean produces widespread "drizzle" evident in Figure 6f. The drizzle occurs at 10^{-3}–10^{-2} mm/day, which corresponds to 10^{-4}–10^{-3} kg/m^2 in any 8 hour span of time; *Barth and Rafkin* [2007] predict such drizzle only produces 10^{-8} kg/m^2, and perhaps the discrepancy results from simplifications of our large-scale condensation scheme. Since precipitating cloud features are present at mid and high summer latitudes during solstices, the 7 m case is also consistent with available cloud observations. Large, episodic outbursts of precipitation at the summer poles can also potentially explain the south-polar cloud outburst seen in ground-based observations by *Schaller et al.* [2006]. The existence of weak but widespread condensation and precipitation in the 7 m case could also be consistent with the precipitating stratiform cloud inferred during the Huygens descent [*Tokano et al.*, 2006b; *Lorenz et al.*, 2007].

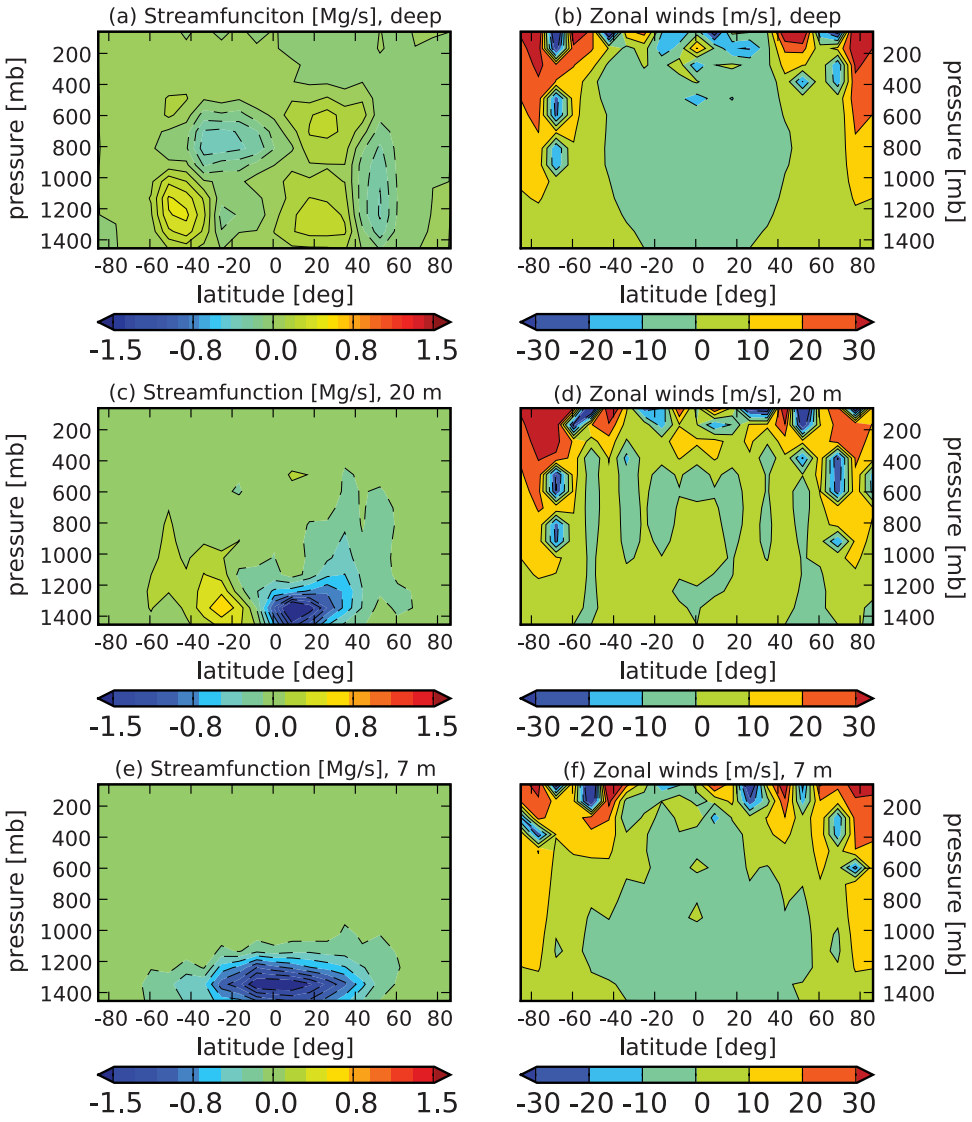

Figure 8. Average mass fluxes in Mg/s (left column) and zonal winds in m/s (right column) for the last four simulated Titan seasons for a subset of our model simulations. Positive (negative) fluxes indicate counterclockwise (clockwise) circulation and positive (negative) zonal winds travel west to east (east to west).

5.2. Large-Scale Circulation

[31] Once completely dry regions form, the soil model self-consistently alters the evaporative flux at the surface. Therefore we expect the resulting large-scale dynamics to have features that can be understood in analogy to the dry and moist simulations by *Mitchell et al.* [2006]. Here we briefly discuss the circulation patterns in these two limiting cases in order to frame subsequent discussion of the terraplanet simulations. We will undertake a more thorough description of the simulations by *Mitchell et al.* [2006] in a separate paper.

[32] Figure 7 shows the annually averaged meridional circulations in the moist and dry cases by *Mitchell et al.* [2006]. Cool colors outlined by dashed lines indicate clockwise motion and warm colors outlined by solid lines indicate counter-clockwise motion. A primary distinguishing feature between these cases is the depth of the overturning circulation. In the moist case, latent heating allows persistent, deep convection which forms a deep overturning circulation that is thermally indirect at low latitudes due to strong, cross-equatorial flow during solstices. In the dry case the convection is shallower, and the resulting circulation is also shallow and significantly more vigorous. (The neutral stability set by dry convection prevailing in the lower atmosphere requires a large mass flux to transport an amount of heat required to keep equatorial temperatures uniform in order to satisfy the angular momentum constraint (see *Held and Hou* [1980] or *Caballero et al.* [2008])). The annually averaged overturning cells in the dry case are hemispherically asymmetric; the asymmetry of the seasonal forcing, which produces a slightly stronger southern summer solstice than northern summer solstice, creates a stronger cross-equatorial circulation at southern summer solstice

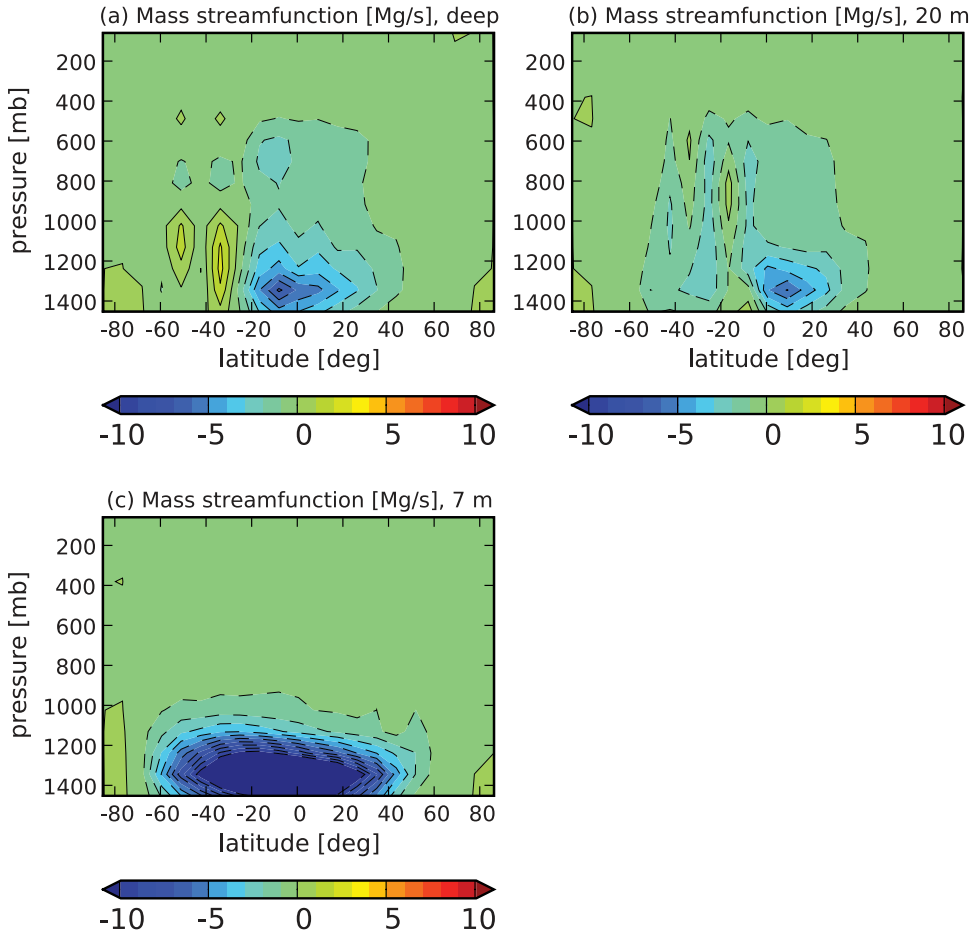

Figure 9. Instantaneous SSS mass fluxes in Mg/s, where positive (negative) fluxes indicate counterclockwise (clockwise) circulation. Note the change in color scale relative to mass fluxes in Figure 8.

compared to northern summer solstice that biases the annual mean.

[33] We expect our terraplanet simulations will have features of both of these limiting cases. If insufficient surface methane is available to produce deep convection during a given season, the circulation will be shallow and vigorous like the dry case. Seasons in which sufficient methane is available to sustain deep, precipitating convection will have deep, sluggish circulations.

[34] Figure 8 shows the annual-mean Hadley circulation (left column) and zonal winds (right column) for our three representative simulations. In the deep case, the four-cell pattern seen in the moist aquaplanet simulation (Figure 7a) is evident, indicating the low-latitudes experience a net downdraft in the annual mean. The associated divergence of surface-level air dries the low-latitude surface. The surface-level convergence at mid latitudes marks the location of the solstitial large-scale updraft, the point at which the circulation is strongest. The zonal wind pattern is mostly easterly in the low latitudes with high-latitude westerly jets in both hemispheres.

[35] In the 20-m reservoir case, the low-latitude circulation below 1000 mbar is thermally direct, with an updraft directly at the equator. This low-level circulation is a few times stronger in the 20 m case than in the deep reservoir case. In the 20 m case, low latitudes have completely dried; when the ITCZ is over these latitudes, a more vigorous circulation forms due to locally dry conditions, as in the dry case shown in Figure 7. The mass flux above the boundary layer is less organized. Deep updrafts reaching into the free troposphere (above 1000 mbar) are apparent at mid latitudes and mark the deepening and strengthening of the ITCZ under solstitial conditions, when the most intense precipitation is evident. The deep updraft can be seen in the southern summer solstice (SSS) instantaneous mass flux shown in Figure 9 when the mass flux is nearly an order of magnitude greater than in the annual-mean. Zonal winds are very similar between the 20 m and deep cases, with high-latitude westerly jets and easterlies at low latitudes, though low-latitude easterlies are not as well-organized in the 20 m reservoir case. We will discuss the origin of this zonal wind pattern in section 5.3.

[36] The mean meridional circulation and zonal winds in the 7-m reservoir case have a much different character than the other cases. The annual-mean mass flux is completely asymmetric, with rising air in the southern hemisphere and descending air in the northern hemisphere. The Hadley cell is responding strongly to the asymmetry in the seasonal

forcing, which is greatest during SSS. The overturning circulation is confined to a shallower layer corresponding to the depth of the dry convective layer in Figure 11a, and it is more vigorous than the other cases, as expected from the dry limit in Figure 7. Only the very highest latitudes have westerly winds, and the zonal winds at low and mid latitudes are nearly static.

[37] In order to develop a more thorough understanding of how the large-scale circulation produces and sustains the zonal winds in these cases we turn to a discussion of the angular momentum transport.

5.3. Angular Momentum Transport

[38] The Hadley cell is fundamental to the large-scale circulation and angular momentum distribution of an atmosphere. Surface-level air is warmed by solar radiation which gives rise to a buoyant updraft. This air travels poleward above the boundary layer in the free troposphere where angular momentum of the zonal mean flow is conserved in the absence of eddy effects and friction. The air cools radiatively until it sinks at a certain latitude; a jet forms at this latitude from the transport of high-angular-momentum air to regions of lower angular momentum. The return branch of the cell travels along the surface where angular momentum from the surface is imparted to the air by friction, and the cycle begins again. The circulation in this picture is steady and thermally direct, i.e., it acts to transport heat down the thermal gradient in latitude [*Held and Hou*, 1980]. While this model provides a good description of angular momentum transport by a steady large-scale circulation, the effect of seasonal oscillations on the angular momentum distribution is not captured.

[39] An accurate approach to analyzing the effect of seasonal oscillation on the momentum budget can be performed by separating the momentum flux into time-mean and time-varying components. This is done by assuming the angular momentum, J, and velocities, $\mathbf{v} = (v,w)$, can be described by a time-mean and a variable component around the mean, $J = \overline{J} + J'$, $\mathbf{v} = \overline{\mathbf{v}} + \mathbf{v}'$, where overbars denote time-averages and primes indicate time-varying components. The time-mean of the angular momentum flux is therefore

$$\overline{\mathbf{v}\mathrm{J}} = \overline{\mathbf{v}}\overline{J} + \overline{\mathbf{v}'J'}. \tag{8}$$

[40] Figure 10 shows the annual-mean vertical (left column) and horizontal (right column) angular momentum flux averaged over the free troposphere (above 1000 mbar). Angular momentum transport in regions that are dominated by the mean-product term ($\overline{\mathbf{v}}\overline{J}$) can be understood as being transported by the annual-mean mass flux (shown in Figure 8), while regions dominated by the time-variable term ($v'J'$) are subject to mixing of angular momentum from the time-varying component of the mass flux. In all plots, positive(negative) fluxes correspond to upward/northward (downward/southward) transport of angular momentum.

[41] The vertical and horizontal momentum fluxes in both the deep and 20-m reservoir cases are dominated by the mean-product term, which reflects a sluggish overturning timescale relative to the seasonal cycle. Angular momentum at the equator in the 20 m case does not reach the free troposphere at the equator despite having an annual-mean updraft located at the equator. This can be understood from the shallowness of the low-latitude annual-mean mass flux in Figure 8, which is largely contained in the boundary layer below 1000 mbar. Deep updrafts are evident in the deep and 20 m cases just poleward of this region where the largest vertical momentum flux is located; this is the flow that injects angular momentum supplied to the boundary layer by surface friction into the free troposphere. The horizontal flow transports this angular momentum poleward to high latitudes where the zonal jets form. Subsidence at high latitudes and at/near the equator returns this air to the boundary layer, where frictional effects transfer the momentum back to the surface. This scenario holds for any regime in which a deep ITCZ oscillates between mid-latitude accumulation zones.

[42] Angular momentum fluxes in the 7-m reservoir case are distinct from the other cases. Figure 10e reveals a region of mean-product-dominated upward angular momentum flux around the equator and near the southern pole and downward flux at mid latitudes. This structure suggests some positive angular momentum is deposited in the free troposphere, giving rise to the high-latitude westerlies seen in Figure 8. The horizontal angular momentum flux in the 7 m case has little discernible structure. The Hadley cell is entirely within the boundary layer in this case, so there is very little horizontal mass flux in the free troposphere to redistribute angular momentum. The layer between 1000 mbar and the tropopause may be subject to 3D effects like barotropic eddies not captured in our 2D model; if so, these effects likely contribute significantly to the angular momentum transport in this layer.

5.4. Surface Temperatures and Surface-Atmosphere Moisture Partitioning

[43] The observed temperature profile is consistent with being in radiative equilibrium with a shallow layer of dry convection near the surface [*McKay et al.*, 1989; *Fulchignoni et al.*, 2005]. This profile, however, may not be representative of areas of moist convection where clouds are formed. The gray line in Figure 11a shows the temperature profile in our model when moist convection is active. The surface temperature in regions of moist convection is lower than radiative equilibrium of our model (dashed line) and the observed temperatures (Huygens—red line; Voyager —blue line). This change in surface temperature does not violate energy conservation because Titan's atmosphere is optically thick to infrared radiation, which decouples the surface and lower atmosphere from the outgoing infrared radiation. On the other hand, the temperature at the radiating layer (where the optical depth measured from the top of the atmosphere equals one) must remain constant at the value that balances the incoming solar radiation. The radiating layer corresponds to about 350 mbar (30 km) in our model. Since the methane moist adiabatic lapse rate (vertical portion of the gray line in Figure 11b) is lower in magnitude than that of the nitrogen dry adiabatic lapse rate (dotted line in Figure 11b), a deeper portion of the column is unstable to moist convection (up to 500 mbar) than to dry convection (up to 1300 mbar). This unstable layer is below the radiating level and is therefore allowed to change without altering energy balance. The resulting surface temperature extrapolated down along the moist adiabat from the temperature at

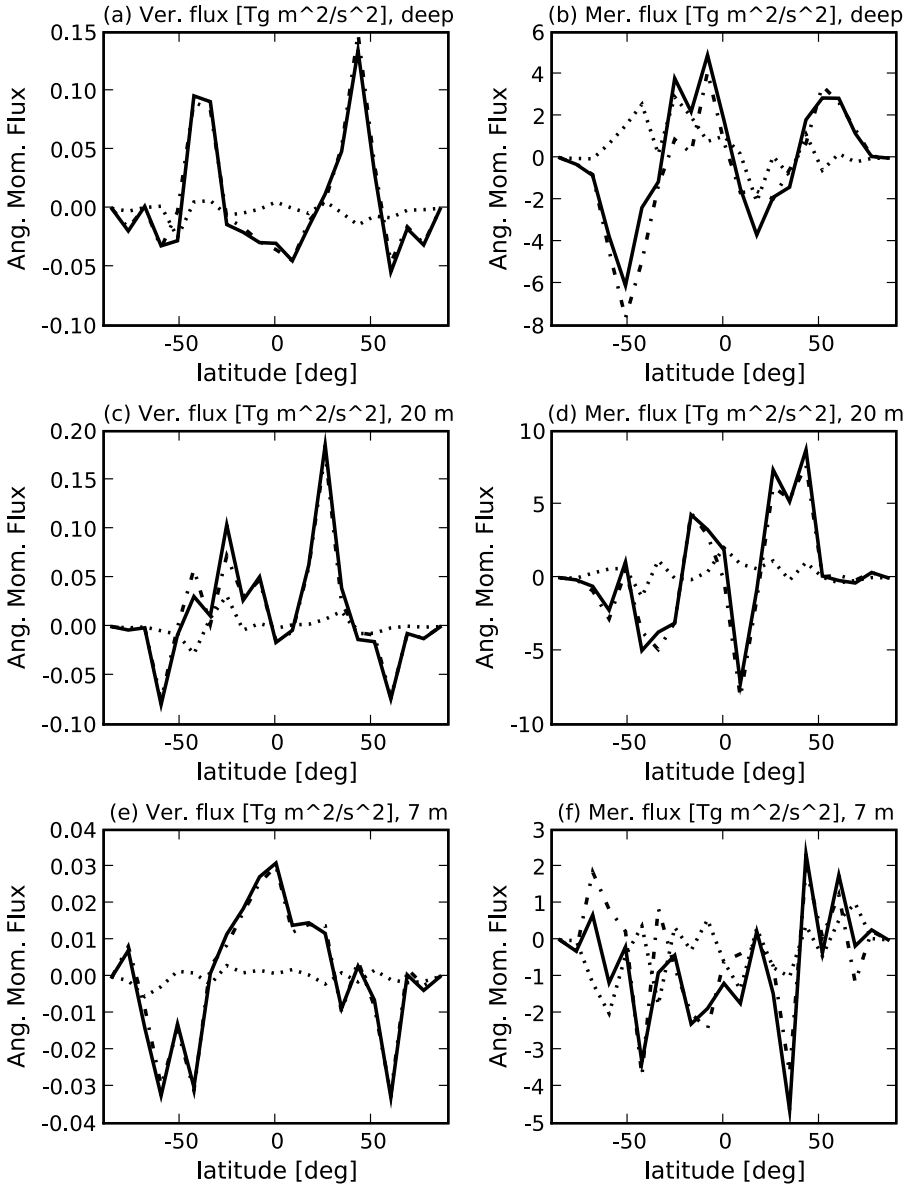

Figure 10. Vertical (left column) and horizontal (right column) momentum fluxes in Tg m^2/s^2 averaged above the 1000 mbar level. Positive (negative) values indicate prograde angular momentum transport either upward (downward) for vertical fluxes or northward (southward) for meridional fluxes. Lines represent the following momentum fluxes: dash-dot line, annual mean; dotted line, time varying; solid, total. Note the different scales on the y-axes; the meridional flux can be up to an order of magnitude larger than the vertical flux.

500 mbar is lower than would exist in radiative or dry radiative-convective equilibrium (see Figure 11a). Surface temperatures in areas of efficient moist convection are depressed by this mechanism. Were we to include the radiative feedback of methane, the temperature difference between the warm, dry convective state and the cool, moist convective state would be more pronounced since in the warmer state the atmosphere contains a higher concentration of methane (see Figure 12b). However, we do not account for the infrared window at around 500 cm^{-1} [*McKay et al.*, 1989], which could affect this mechanism by allowing a small portion of the infrared radiation from the surface to escape directly to space, coupling the surface temperature to the outgoing longwave radiation.

[44] Figure 12a shows the annual-mean surface temperatures for our three cases. The deep reservoir (black line) and 20 m reservoir (dashed line) cases are clearly in a cool, moist regime; surface temperatures in these cases are around 90 K at low latitudes and drop to 87 K at the poles. The surface temperatures in the deep and 20 m cases change each year by around 5 K in most locations, with the most pronounced changes occurring at high latitudes. The dried regions in the 20 m reservoir case produce slightly enhanced surface temperatures between 20N and 20S and near 60N/S in the annual mean. In this region, shallow, dry convection allows higher surface temperatures by the mechanism explained in the preceding paragraph. The annual-mean surface temperatures are at or just below the freezing point

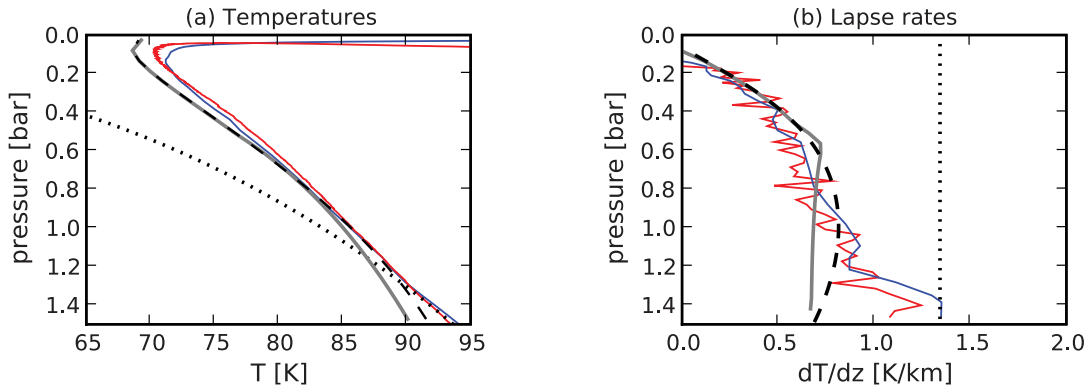

Figure 11. (a) Temperature profiles and (b) lapse rates for radiative equilibrium of our model (dashed line), moist radiative-convective equilibrium of our model (solid gray line), the observed Huygens temperature profile (solid red line), and the observed Voyager temperature profile (solid blue line, reproduced from data in Table 1 of *Lindal et al.* [1983]. The dry nitrogen adiabat starting at the observed surface temperature and corresponding lapse rate are also shown (dotted line).

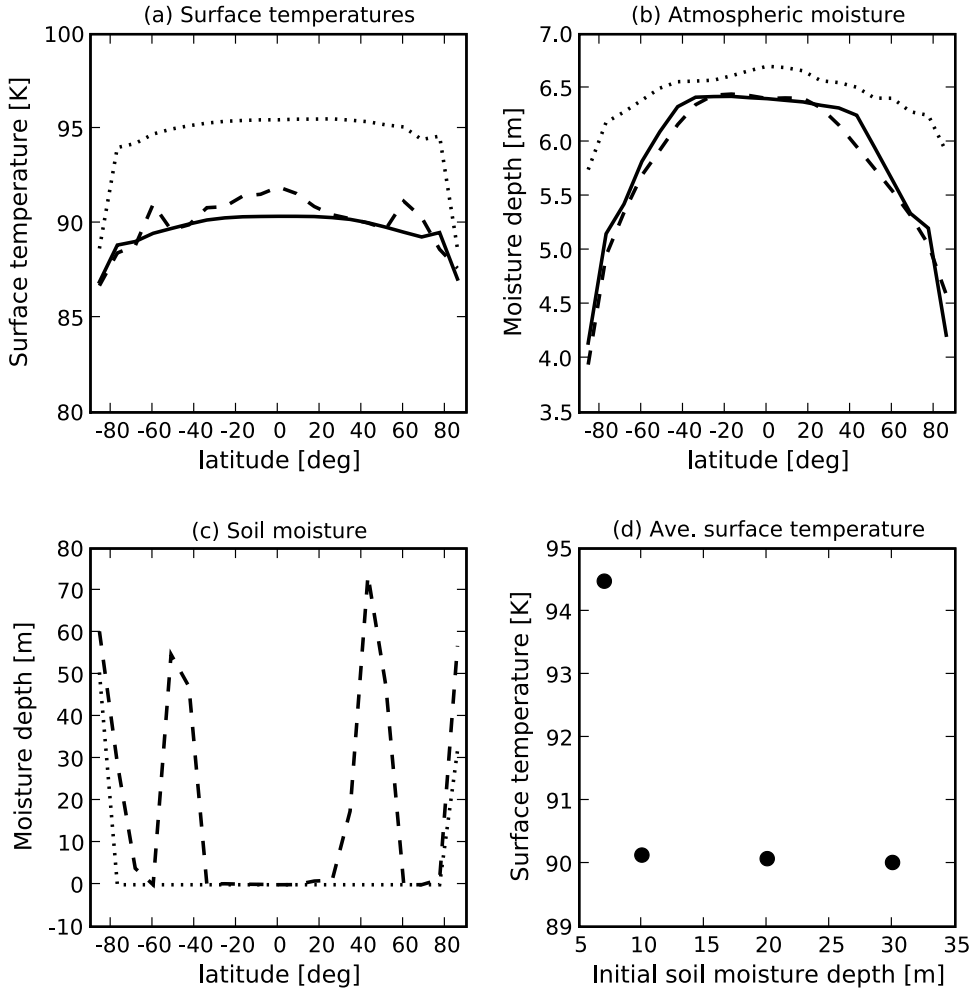

Figure 12. (a) Annual-mean surface temperatures vs. latitude. (b) Atmospheric moisture depth vs. latitude. (c) Soil moisture depth vs. latitude. (d) Horizontal-mean temperatures vs. initial reservoir depth. The line styles indicate the following: deep reservoir case, solid line; 20-m reservoir case, dashed line; 7-m reservoir case, dotted line.

of methane, so one might expect ice to form in these cases. Instantaneous surface temperatures, however, are higher than the annual mean (especially over the dry regions, not shown), and are at or above the freezing point. We do not account for freezing of methane in our model, which could affect our results by significantly reducing the evaporative surface flux. Surface temperatures below the freezing point occur mostly in the winter hemisphere, where there is very little evaporation occurring (see Figures 4 and 5). We performed a simplified sensitivity test by shutting off evaporation in regions where the surface temperature drops below freezing (90.67 K). Since surface evaporation is strongly confined to the summer regions which are above freezing, we found this has almost no effect on our results. One should more accurately account for the freezing by including the latent heat of fusion/melting of methane, which would require a model for the growth of ice in some assumed type of surface reservoir. The latent effects could change our results by adding thermal inertia to the surface. If the liquid methane is not pure, its freezing point will generally be depressed. *Mitri et al.* [2007] show that if the mole fraction of methane is 35% in surface liquids (the balance being mostly ethane), the freezing temperature of methane is depressed by 2.5 K while the vapor pressure of methane is reduced by a factor of 0.35. The latter case is similar to the intermediate case by *Mitchell et al.* [2006], which we will discuss in the context of terraplanet simulations in a future paper.

[45] The 7-m reservoir case is in an entirely different regime, with elevated surface temperatures everywhere, as Figure 12a shows. Annual-mean, low-latitude surface temperatures in this case are more consistent with the ~94 K observed by Huygens [*Fulchignoni et al.*, 2005]. Surface temperatures change by around 5 K at most latitudes, but the most extreme changes happen at high latitudes which is qualitatively similar to the results for a "porous icy regolith" by *Tokano* [2005] (Figure 1). Temperatures below the freezing point of methane are limited to the winter pole, though this may have a significant effect since the liquid reservoir in this case occurs at the poles. The transition to this dry, warmer state is abrupt as the reservoir depth is varied. The reason for this strong threshold behavior can be understood by comparing the reservoir size to the moisture content of the atmosphere. Figure 12b shows the annual-mean equivalent liquid methane depth of the methane vapor in our model atmospheres. In the cooler, moist regime, the atmosphere has 6.3 m of liquid methane equivalent in vapor form. In the 7 m case, higher surface and low-level temperatures dictate higher saturation vapor pressures, and the moisture content of the atmosphere increases. The transition to this warmer regime occurs when the initial reservoir depth is near the level of atmosphere moisture storage; when the atmosphere can store most of the initial reservoir, the surface must become very dry, which results in warmer temperatures that positively reinforces this warming/drying process. Figure 12c shows the annual-mean soil moisture in the 20 m and 7 m cases. The 7 m case is unable to sustain mid-latitude accumulation zones as in the 20 m case. Though the polar zones accumulate deep reservoirs in the 7 m case, the actual mass of surface methane at these latitudes is quite small, and most of the moisture is contained in the atmosphere.

5.5. Atmospheric Temperature and Methane Vapor Concentration

[46] The annual-mean atmospheric methane vapor concentration in g/kg and temperature in K for each of the three cases are displayed in Figure 13. In the deep reservoir (Figures 13a and 13b) and 20 m reservoir (Figures 13c and 13d) cases, methane vapor is most strongly concentrated over low latitudes. In the latter case, there is a slight enhancement in vapor concentration over the edges of the dried region from 20N to 20S, suggesting surface dryness only locally depresses atmospheric vapor concentration. The overall character of the methane distribution is consistent between these cases, which corroborates the similarity of other aspects of these simulations.

[47] The plots of atmospheric temperature show the Hadley cell's ability to homogenize the temperature structure, as is expected from theory [*Held and Hou*, 1980]. The annual-mean horizontal temperature gradient is confined primarily to latitudes poleward of 50N/S. At latitudes equatorward of 50 N/S where temperatures are horizontally uniform, decreasing methane vapor concentrations moving from the equator to either pole signal a decrease in the saturation ratio, which is defined as the ratio of the vapor concentration to the saturation concentration. Near the poles where temperatures drop significantly, the saturation ratio increases because the drop in the saturation concentration, which exponentially increases with temperature, overtakes the drop in the methane concentration. Because of this strong temperature dependence, the columns of air above poles have the largest annual-mean saturation ratios (not shown).

[48] Temperatures and methane concentrations in the 7 m reservoir case (Figures 13e and 13f) are significantly different from the other two cases. Methane vapor concentrations are very uniform below 1000 mbar (roughly 8 km altitude) and equatorward of 80N/S. Moisture homogenization is not due to the boundary layer diffusion, which is very weak in these simulations. Rather, the circulation is reorganizing methane vapor without producing significant precipitation, such that methane vapor is mixed as a nearly passive tracer in this region. The largest methane concentrations occur near the surface over the poles, which is the only region where surface methane is persistently available (see Figure 4c). Temperatures are made even more uniform than the 20 m and deep cases by stronger oscillations and larger mass fluxes than in the other two cases, and as a result horizontal temperature gradients are confined poleward of 80 N/S. Because of the uniformity of temperature and methane vapor, the saturation ratio is horizontally uniform near the surface over much of the globe. Saturated air near the polar surface is mixed throughout the region between 80N to 80S by the oscillating Hadley circulation, and a temperature increase of a few Kelvin toward the equator is sufficient to change saturated, polar air to below 50% saturation ratio at low latitudes, as was observed by Huygens [*Niemann et al.*, 2005]. Our 7 m reservoir case confirms the mechanism suggested by *Mitri et al.* [2007] for depressed relative humidity at low latitudes: the circulation can sustain intermediate humidities even if the surface liquids are confined to a very small area.

[49] In each of the cases, there is temporal variability in the local methane vapor concentration (not shown). In the deep and 20 m cases, the most variability is seen in the mid

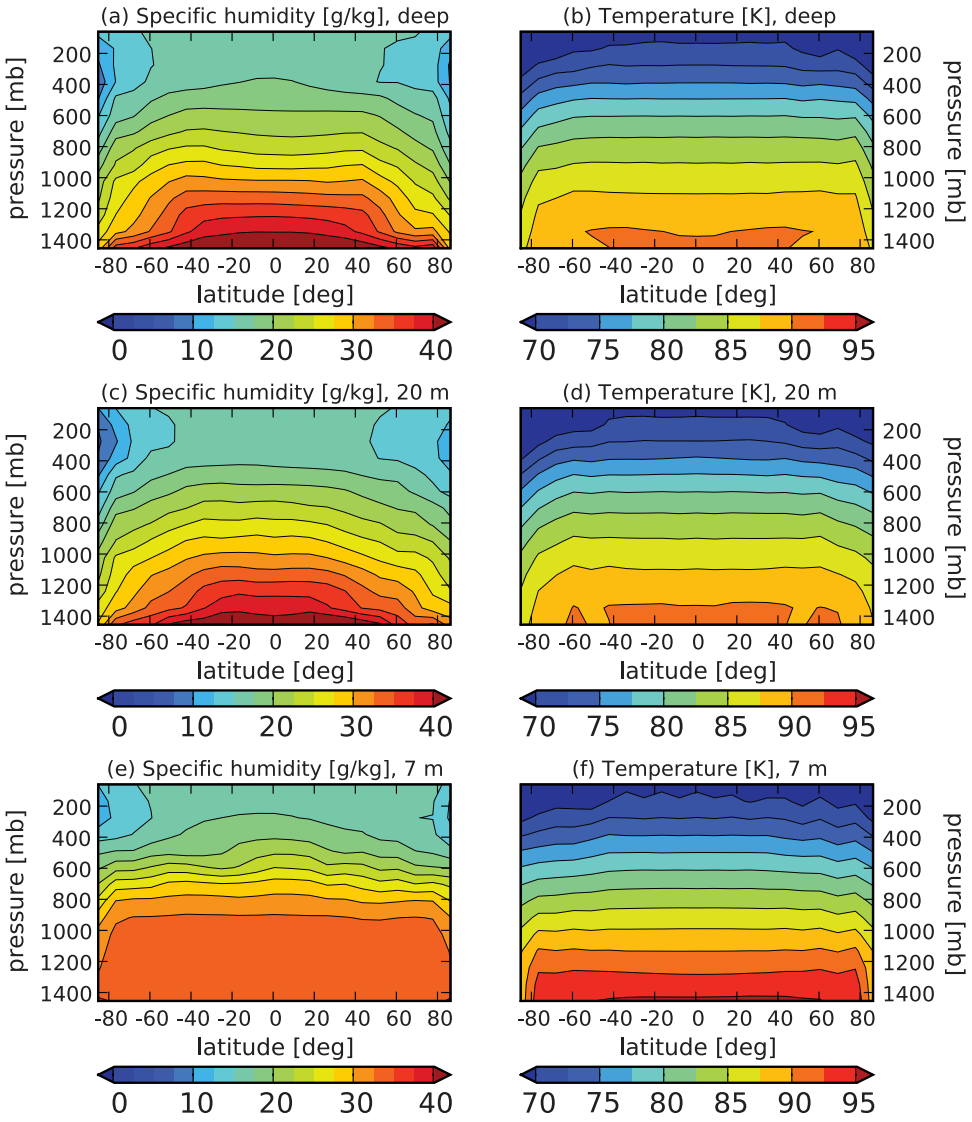

Figure 13. Annual-mean atmospheric specific humidity in g/kg (left column) and temperature in K (right column).

and low latitudes, where convection is locally very seasonal due to the oscillating ITCZ. The near-surface air parcels in these cases typically vary 10–15 g/kg during the course of a Titan year. In the 7 m case, the mid- and low-latitude methane vapor concentration does not significantly vary from the annual-mean. Rather, the polar regions experience the most variation in methane concentration; near the ground the concentration is 15 g/kg higher during the summer months than in the winter months.

6. Comparison With Observations

[50] The zonal wind profile observed by Huygens showed westerlies aloft in a region roughly equivalent to the free troposphere (above 1000 mbar) of our model [*Bird et al.*, 2005]. Below this level, winds reverse direction and become weak easterlies. The right column of Figure 8 shows the annual-mean zonal winds in our three representative simulations (instantaneous winds are not significantly different); weak easterlies prevail at low latitudes in the free troposphere in the deep reservoir limit, while some patchiness between weak easterlies and westerlies develops over dried regions in the 20 m and 7 m reservoir cases. The oscillating Hadley cell does not allow strong, low-latitude westerlies to form in our angular-momentum-conserving, zonal-mean model, since easterly momentum is transported equatorward from deep mid- or high-latitude updrafts at solstices. Our simulations are, therefore, inconsistent with the observed Huygens zonal wind profile. However, when the Hadley cell is over dry regions, it is confined primarily to the boundary layer, and the vertical transport of angular momentum into the free troposphere at low latitudes by the Hadley cell is limited. This shallow Hadley cell occurs in the 20 m reservoir case when the ITCZ is between 20 N/S and over much of the globe in the 7 m reservoir case. Without the influence of angular momentum transport by the Hadley cell, low-latitude zonal winds in the free troposphere are very sensitive to a variety of radiative, convective, and dynamic phenomena. If the Hadley circulation on Titan is persistently shallow, the Huygens obser-

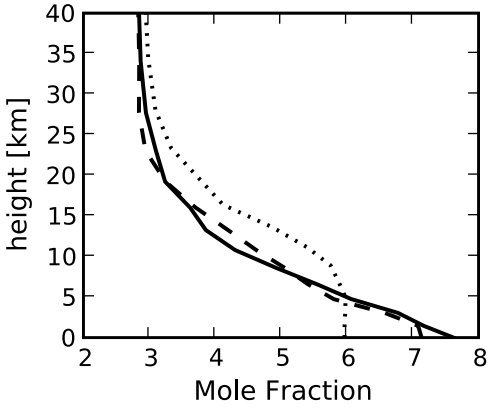

Figure 14. The profile of methane mole fraction (%) with altitude at the epoch when and location where Huygens descended through Titan's atmosphere in our three cases. Deep reservoir, solid line; 20-m reservoir, dashed line; 7-m reservoir, dotted line.

vations could be a signature of a low-latitude wave carrying westerly momentum that happened to form at this particular epoch. If instead low-latitude westerlies prevail at all times, the westerly jets at high latitudes must supply momentum to low latitudes by some eddy process which is not captured in our model. For instance, barotropic eddies that transport momentum but very little heat could mix momentum from high-latitude jets equatorward, as they do in the stratosphere (see e.g., *Hourdin et al.* [1995]).

[51] *Mäkinen et al.* [2006] derived the vertical wind from the Huygens descent, which showed rising motion through the depth of the troposphere below 40 km. None of our simulations produce rising motion at low southern latitudes during the Huygens epoch above 10 km. However, the 7 m case does produce rising motion at the Huygens descent location and epoch in the lowest several kilometers. The Hadley cell in the 7 m case during the Huygens epoch is a single, cross-equatorial circulation confined to the lowest ~10 km. The updraft and downdraft of the dry Hadley circulation are roughly equal in area, in contrast to Hadley cells in the presence of moist convection (the deep and 20 m cases) which have much narrower updrafts than downdrafts. The large latitudinal extent of the dry Hadley cell updraft creates upwelling at all summer latitudes at the Huygens epoch. The layer between 10 and 40 km has little or no motion in the 7 m case. As we pointed out in the context of zonal wind observations, the intermediate layer between 10 and 40 km could be strongly influenced by mechanisms not captured by our model. The fact that our 7 m case is consistent with the observed vertical winds in the lowest layer further suggests this case is most consistent with observations.

[52] The vertical profile of methane concentration observed by Huygens at low latitudes showed the upper troposphere is roughly saturated (decreasing mixing ratio with height) while methane below 8 km (~1000 mbar) is well-mixed at a constant mole fraction of 5%; because of increasing temperatures from 8 km to the ground, the saturation ratio of methane decreases to below 50% near the ground [*Niemann et al.*, 2005]. Figure 14 shows the vertical profile of methane mole fraction, which is approximately the mass mixing ratio (specific humidity) divided by the ratio of the mean molecular weights of methane and molecular nitrogen, for our three simulations (We plot mole fraction in order to make a direct comparison with Figure 2 of *Niemann et al.* [2005].). In the deep and 20 m reservoir cases, the methane mole fraction decreases monotonically with height, which roughly keeps the saturation ratio fixed as temperatures decrease with height. The 7 m reservoir case is more consistent with observations, with decreasing mole fraction with height in the upper troposphere and roughly constant mole fraction in the lowest several kilometers (The value of the mole fraction is somewhat higher than observed because the surface temperature at this location is somewhat warmer than observed, but the resulting humidity is ~45%, as observed.) As previously noted, methane is passively transported from saturated conditions near the poles to the warmer low latitudes, which sustains the uniform concentration in the lowest several kilometers. Again, the 7 m reservoir case is most consistent with the observed vertical profile of methane.

[53] The total column depth of methane observed by the Huygens probe is equivalent to ~5 m of liquid methane [*Tokano et al.*, 2006b]. All of the scenarios presented here have column depths slightly larger (~6.5 m) than observations at low latitudes (see Figure 12b). This modest discrepancy could be due to elevated model temperatures, relative humidities, or both. In the deep and 20 m cases, the relative humidities near the surface are higher than observed, while in the 7 m case temperatures near the surface are slightly elevated and humidities are consistent with observations.

[54] *Tokano et al.* [2006b] showed evidence for a stratiform cloud around 20 km altitude in the Huygens descent data producing a "drizzle" at low latitudes; Huygens was also buffeted by turbulence in this layer, likely marking the presence of condensation between 20 and 30 km altitude [*Lorenz et al.*, 2007]. This type of cloud is most consistent with large-scale condensation in our model, which is produced at around 25 km (400 mbar) during the Huygens epoch in the 7 m reservoir case (the features in the annual mean in Figure 6 reflect precipitation at nearly all times). However, the 7 m case does not produce deep, mid-latitude convective clouds of the type that have been observed [*Roe et al.*, 2005a; *Griffith et al.*, 2005], while simulations with deeper reservoirs retain mid-latitude convective precipitation. *Roe et al.* [2005b] argue the longitudinal localization of mid-latitude clouds can only be explained by localized surface sources (such as cryovolcanoes), which suggests the 7 m reservoir case could still be consistent if this mechanism were introduced into our model. However, *Porco et al.* [2005] claim the distribution of mid-latitude clouds is uniform in longitude, suggesting they are produced by large-scale dynamics.

7. Discussion and Interpretation

[55] The uncertainty in the mechanism producing the observed clouds may be resolved by future observations of clouds as the Titan season progresses towards an equinox. If the convective clouds move equatorward, our simulations suggest dynamics are responsible for creating them, and the 7 m case would be inconsistent with observations. Alternatively if convective clouds disappear during

equinoctial conditions or remain at southern mid latitudes, the deeper reservoir (10 m and above) cases would be inconsistent with observations. However, some other combination of cloud phenomena may be observed, in which case a different interpretation would be required.

[56] Surface conditions at the Huygens landing site are consistent with a sandy material wetted with liquid methane below a crust of solid material [*Zarnecki et al.*, 2005]. This crust likely isolates the methane from evaporating into the atmosphere, but it is unclear if this is a permanent feature or representative of the current seasonal conditions at low latitudes. If precipitation is strong enough at a different season, for instance, the "methane table" might reach the surface and locally resupply the atmosphere with evaporated methane, allowing convective clouds to form. Or perhaps the subsurface methane travels in an underground "methanafer" which accesses the surface at different locations. If such effects were taken into account in our model, we might expect the drying threshold seen in our simulations around 7 m reservoir depth would become less abrupt. Instead, the transition regime could take on desirable features of both the 20 m reservoir case, like deep convective precipitation at mid and high latitudes during solstices, and the 7 m reservoir case, like low-latitude stratiform clouds during solstices and a well-mixed layer of atmospheric methane. While these effects are not captured in our current model, they could be explored with simple modifications.

[57] *Atreya et al.* [2006] suggest methane formed in the interior of Titan and outgassed to the surface by volcanism could roughly balance the photochemical destruction of methane in the stratosphere. *Tobie et al.* [2006] claim that over geologic time, the outgassing of methane from clathrate hydrates occurred in episodic bursts, followed by a slow decay and cutoff in the outgassing rate; by their model, methane is currently outgassed at a decaying rate approaching the photodissociation rate such that the methane reservoir could be shrinking. *Lopes et al.* [2007] show several cryovolcanic surface features observed by Cassini which are thought to support methane outgassing during the current stage of mantle convection. If the methane inventory is evolving with time, some surface erosion features could exist from an earlier climate epoch when the methane inventory was larger. For instance, the appearance of fluvial erosion features at low latitudes embedded in areas primarily covered by dunes might indicate a wetter climate that existed following a large methane outgassing event, but one must then explain why the material from surrounding dunes has not buried these features. A thorough investigation of the interaction between the long-term evolution of the methane inventory and mechanisms in the climate that redistribute the reservoir require a simpler model which can be run for very long time periods, and we intend to explore this in future work. Alternatively, the seasonal variation of the ITCZ could cause precipitation over the same regions each season, but no mechanism existing in models allows precipitation to preferentially and repeatedly form at specific locations.

8. Conclusions

[58] We developed a novel model of Titan's climate that takes into account redistribution of a limited methane reservoir in the surface-atmosphere system. The model consists of an atmosphere coupled to a simplified soil surface model. The soil model is made of a grid of "buckets" covering the entire surface. Each bucket has an infinite capacity to store liquid, which eliminates the redistribution of surface liquids; in this sense, it represents the opposite limit to that assumed in previous studies in which the surface has an infinite supply of and therefore capacity to redistribute moisture [*Tokano et al.*, 2001; *Rannou et al.*, 2006; *Mitchell et al.*, 2006]. We performed simulations with varying amounts of initial methane in order to explore the feedbacks between surface drying, large-scale dynamics, and precipitation. All simulations produce net drying of the low-latitude surface from a seasonally oscillating Hadley circulation.

[59] We began by establishing the low-latitude drying rate of our model by performing a simulation with an initially very deep methane reservoir. We found low latitudes (roughly between 20 N/S) dry by $\sim$1.75 m of liquid methane per Titan year due to low-latitude methane vapor divergence by the large-scale circulation. Observations of the low-latitude surface suggest dry conditions prevail [*Lorenz et al.*, 2006] which indicate the methane inventory with access to the atmosphere has had sufficient time to be removed from the low latitudes by this mechanism; additional information on the time during which the methane inventory has been in steady state is required to estimate the size of the methane reservoir. We then explored initial methane reservoirs of 30 m, 20 m, 10 m, and 7 m; initial reservoir depths above 10 m all produced similar results which are analogous to the moist simulation by *Mitchell et al.* [2006], while the 7 m reservoir case showed evidence of a much different regime. We narrowed our focus further to the deep, 20 m, and 7 m reservoir cases, and analyzed these simulations in detail.

[60] The deep and 20 m reservoir cases were similar in most respects, including annual-mean mass fluxes, angular momentum transport, surface and atmospheric temperatures, and atmospheric methane concentrations. These cases resembled the moist simulation by *Mitchell et al.* [2006], except for differences in the annual-mean Hadley cell attributable to the change in radiative regime and boundary layer parameters.

[61] The 7 m reservoir case is in an entirely different regime which resembles the dry simulation by *Mitchell et al.* [2006]. The annual-mean Hadley cell is shallow, primarily confined below the 1000 mbar level, and asymmetric about the equator. Dry surface conditions over most of the globe constrain convective areas to the dry adiabat. The steep lapse rate of the dry adiabat creates higher surface temperatures than in the other cases. Higher temperatures allow more methane to be stored as vapor in the atmosphere, which creates a very abrupt transition to this regime; the transition occurs when the atmosphere can roughly store the total methane reservoir, which is equivalent to a uniform, global 6.5 m initial methane reservoir.

[62] The vertical profile of methane vapor concentration in the 7 m reservoir case most resembles that observed by Huygens, with saturated air aloft and constant mixing ratio in the lowest several kilometers. Since precipitation only occasionally occurs at mid and low latitudes, methane vapor is effectively a passive tracer which is efficiently mixed by

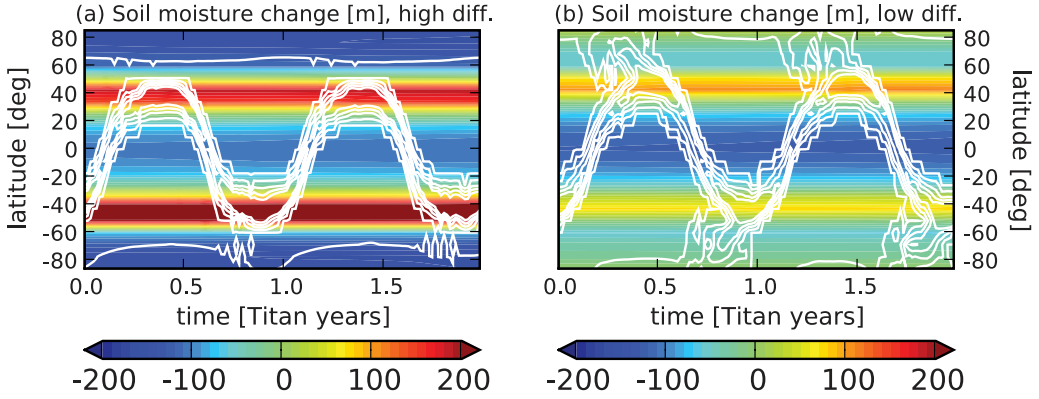

Figure A1. Change in soil moisture depth in meters from the initial, uniform depth (solid contours), and precipitation (open contours) over the last two model years of deep (1×10^6 m) reservoir simulations with two different values of boundary layer diffusion, ν_v.

the Hadley circulation. We conclude that widespread, dry surface conditions resulting from an oscillating Hadley circulation redistributing a limited methane reservoir sufficiently explains the methane concentrations observed at low latitudes by Huygens.

[63] The existence of low-latitude stratiform clouds and mid-latitude convective clouds during the current season suggest Titan's climate may be a hybrid between our 7 m and 20 m reservoir cases. Our current soil model does not take into account the effect of diverse surface types on the redistribution of surface methane, and this diversity could plausibly allow a hybrid case to form. Modifications of our surface model can be made to account for this effect, and we plan to do so in future work.

[64] Low-latitude zonal winds in the free troposphere (above 10 km altitude) are easterly in all cases, making them inconsistent with the observed Huygens zonal wind profile. Our model robustly predicts easterlies all the way to the low-latitude surface in all cases. The observed winds between 10 and 1 km altitude are easterly [*Bird et al.*, 2005], but winds in the lowest km are westerly [*Folkner et al.*, 2006]. None of our scenarios reproduce prograde winds at the surface. Observed upwelling winds in the lowest 40 km [*Mäkinen et al.*, 2006] are marginally consistent with our 7 m case and inconsistent with all others. The shallow large-scale circulation and stable, radiative-equilibrium temperature structure above the boundary layer in the 7 m reservoir case isolates the free troposphere from the angular momentum of the surface. As a result, processes other than angular momentum transport by the large-scale circulation probably produce and sustain the zonal winds aloft. Likely mechanisms include momentum mixing by barotropic eddies and thermal tides. Simple tests of these mechanisms could be performed using a three-dimensional atmospheric model with an assumed basic state and idealized forcing. We plan to undertake a thorough investigation of these mechanisms in future work.

Appendix A: Sensitivity of Model Simulations to Boundary Layer Diffusion

[65] In the high diffusion case, $\nu_v = 1$ m^2/s, polar precipitation does not form robustly at solstices, as can be seen in Figure A1a. In the absence of convection that produces this precipitation, an updraft no longer forms at the poles. Large-scale subsidence dominates the polar regions, which dries the surface by evaporation and moisture divergence. The mid latitudes receive the most precipitation, accumulating deep reservoirs of surface methane, while both low and high latitudes are dried by moisture divergence. Low latitudes are dried by 50+ m, while high latitudes are dried considerably more. (One must remember the mass of soil moisture goes as the soil moisture depth times the cosine of latitude. When one takes this into account, low latitudes lose more mass of moisture than the high latitudes.) The annual-mean mass flux in Figure A2a has weak, thermally indirect cells at low latitudes and direct cells poleward between mid latitudes and the poles.

[66] In the low diffusion case, $\nu_v = 0.01$ m^2/s, polar precipitation does form robustly at solstices, and high latitudes experience net accumulation, as shown in Figure A1b. Low latitudes experience drying of similar magnitude to the high-diffusion case; the magnitude of low-latitude drying is insensitive to the choice of boundary layer diffusion coefficient. These features are desirable since clouds have been most frequently observed at the solstitial pole [*Roe et al.*, 2002], lakes have only been observed at high latitudes [*Stofan et al.*, 2007], and low latitudes are covered with desert-like dunes [*Lorenz et al.*, 2006]. Features of the large-scale circulation change in the low-diffusion case, but not significantly. Figure A2b shows the annual-mean mass flux for the low diffusion case; both the low-latitude indirect cells and high-latitude direct cells are apparent, but the mass flux is weaker in the lowest layers.

[67] Figures A2c and A2d show the instantaneous mass fluxes at southern summer solstice (SSS), which are an order of magnitude larger than in the annual-mean; the northern spring equinox (NSE) mass flux is of similar magnitude to the SSS mass flux (not shown). Since the magnitude of the annual-mean is an average over two solstitial cells of greater magnitude, slight changes in the strength of the solstitial overturning can change the orientation of the annual-mean, low-latitude cells. The SSS, cross-equatorial mass flux (blue contours) is slightly more intense and better-organized in the high-diffusion case than in the low-diffusion case. These features give rise to the

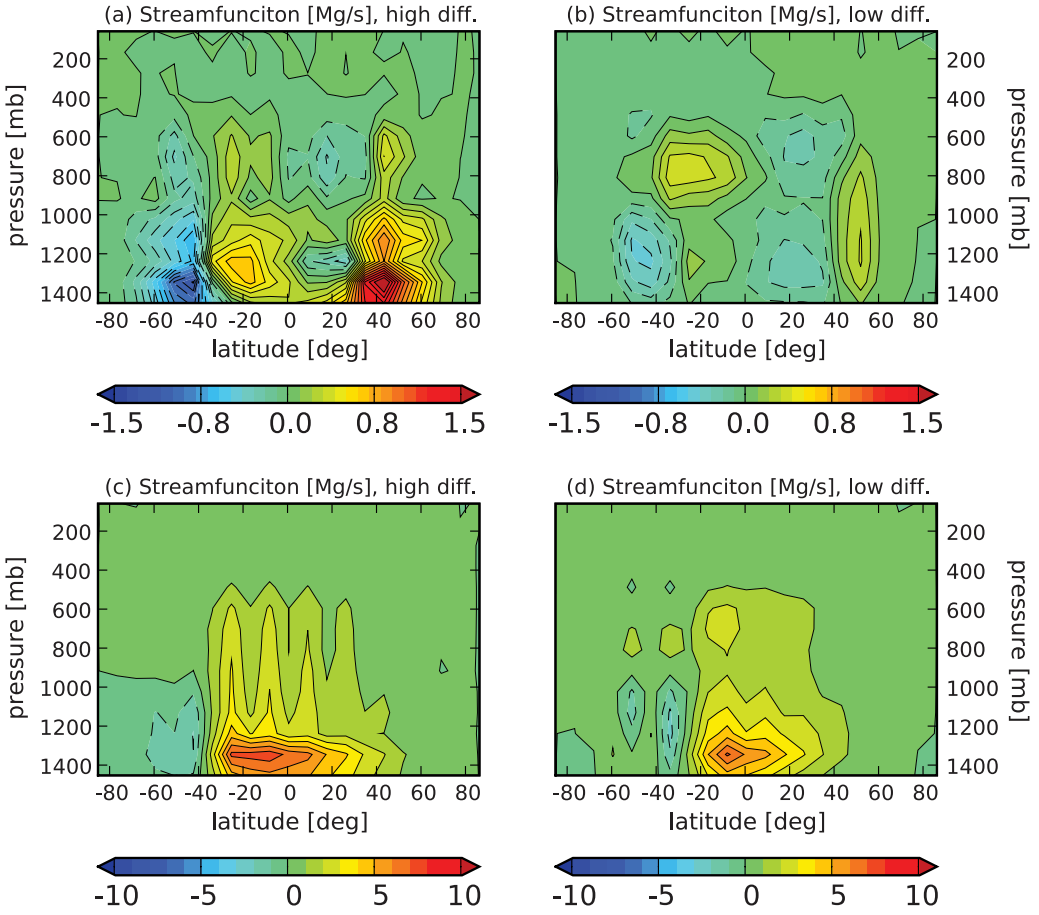

Figure A2. Annual-mean and SSS mass flux in Mg/s for two different values of boundary layer diffusion, ν_v: "high" corresponds to $\nu_v = 1$ m^2/s and "low" corresponds to $\nu_v = 0.01$ m^2/s.

discrepancies seen in the annual-mean mass fluxes between cases, most notably the indirect circulation at low latitudes and high-latitude surface drying in the high-diffusion case.

[68] Momentum damping in the boundary layer is the cause of the change in character of the high-latitude meridional circulation, but in an indirect manner. The annual-mean meridional momentum tendencies averaged over the boundary layer of the high- and low-diffusion cases are shown in Figures A3a and A3b, respectively. In the low-diffusion case, the meridional momentum balance in the high-latitude boundary layer is cyclostrophic, particularly at the south pole; meridional pressure gradients (dashed line) are primarily in balance with the nonlinear advection term (dotted line), $u^2/a \tan(\varphi)$. In the high-diffusion case, meridional momentum is closer to geostrophic balance, with the Coriolis term (solid line) balancing pressure gradients (dashed line). In neither case is the frictional damping term a dominant contributor to the

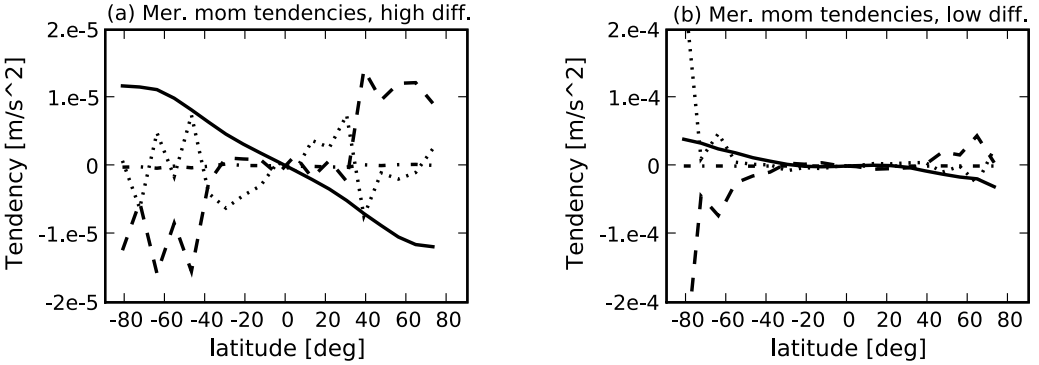

Figure A3. Boundary-layer-averaged, annual-mean meridional momentum tendencies in m/s^2 for two different values of boundary layer diffusion, ν_v, as defined in Figure A2. Lines correspond to the following accelerations: solid line, Coriolis; dashed line, pressure gradient; dash-dot line, diffusion; and dotted line, nonlinear advection.

meridional momentum balance. However, the boundary layer diffusion term (dash-dot line) dominantly contributes to the zonal momentum balance (not shown); in the low-diffusion case, solstitial zonal winds, u, in the boundary layer near the pole reach 15 m/s, while in the high-diffusion case they are damped below 5 m/s, which has a large effect on the metric term, $u^2/a \tan(\varphi)$, in the meridional momentum budget. The reduction of zonal winds from an increase in boundary layer diffusion changes the meridional momentum balance from cyclostrophic to geostrophic. Near solstices, surface temperatures generally decrease from the mid-latitude ITCZ to the solstitial pole (not shown). In the high-diffusion case, geostrophic balance sustains a thermally direct summer Hadley cell near the solstitial pole, surface winds diverge moisture away from high latitudes, and as a result high latitudes experience net drying as seen in Figure A1a. In cyclostrophic balance, an indirect circulation is allowed to form at the solstitial pole and surface winds converge moisture to the poles where net accumulation is seen in the low-diffusion case, Figure A1b. Cyclostrophic flow near the poles is necessary to sustain net accumulation in polar regions, which only occurs in the low-diffusion case.

[69] Our primary goal in this work is to demonstrate the drying of low-latitudes by an oscillating Hadley cell, which we found is robust to changes in the boundary layer diffusion, while maintaining consistency with other observables. Ubiquitous solstitial polar clouds argue for studying a regime in which solstitial polar precipitation is present, which requires us to use low boundary layer diffusion. Furthermore, weak boundary layer diffusion is supported by an analysis of Titan's temperature structure [*Tokano et al.*, 2006a] which suggests a value of v_v is of order 10^{-2} m^2/s.

[70] **Acknowledgments.** I gratefully acknowledge Raymond Pierrehumbert for his guidance on this project, Ralph Lorenz for contributing interpretation of the modeling results in light of Cassini observations, and Dargan Frierson and Rodrigo Caballero for assistance in model development and careful editing of the draft. I also thank Tetsuya Tokano and Erika Barth for thorough reviews of the original manuscript. I gratefully acknowledge support by US National Science Foundation grant ATM-0121028.

References

Atreya, S. K., E. Y. Adams, H. B. Niemann, J. E. Demick-Montelara, T. C. Owen, M. Fulchignoni, F. Ferri, and E. H. Wilson (2006), Titan's methane cycle, *Planet Space Sci.*, *54*(12), 1177–1187.

Barth, E. L., and S. C. R. Rafkin (2007), Trams: A new dynamic cloud model for Titan's methane clouds, *Geophys. Res. Lett.*, *34*, L03203, doi:10.1029/2006GL028652.

Barth, E. L., and O. B. Toon (2006), Methane, ethane, and mixed clouds in Titan's atmosphere: Properties derived from microphysical modeling, *Icarus*, *182*(1), 230–250.

Bird, M. K., et al. (2005), The vertical profile of winds on Titan, *Nature*, *438*(7069), 800–802.

Caballero, R., et al. (2008), Aximmetric, nearly-inviscid circulations in non-condensing radiative-convective atmospheres, *Quat. J. Roy. Meteor. Soc.*, doi:10.1002/qj.271, in press.

Folkner, W. M., et al. (2006), Winds on Titan from ground-based tracking of the Huygens probe, *J. Geophys. Res.*, *111*, E07S02, doi:10.1029/2005JE002649.

Frierson, D. M. W. (2007), The dynamics of idealized convection schemes and their effect on the zonally averaged tropical circulation, *J. Atmos. Sci.*, *64*(6), 1959–1976.

Fulchignoni, M., et al. (2005), In situ measurements of the physical characteristics of Titan's environment, *Nature*, *438*(7069), 785–791.

Garratt, J. R. (1992), *The Atmospheric Boundary Layer*, Cambridge Univ. Press, New York.

Griffith, C. A., et al. (2005), The Evolution of Titan's Mid-Latitude Clouds, *Science*, *310*, 474–477, doi:10.1126/science.1117702.

Griffith, C. A., et al. (2006), Evidence for a polar ethane cloud on Titan, *Science*, *313*(5793), 1620–1622.

Held, I. M., and A. Y. Hou (1980), Non-linear axially-symmetric circulations in a nearly inviscid atmosphere, *J. Atmos. Sci.*, *37*(3), 515–533.

Hirtzig, M., A. Coustenis, E. Gendron, P. Drossart, M. Hartung, A. Negrão, P. Rannou, and M. Combes (2007), Titan: Atmospheric and surface features as observed with nasmyth adaptive optics system near-infrared imager and spectrograph at the time of the Huygens mission, *J. Geophys. Res.*, *112*, E02S91, doi:10.1029/2005JE002650.

Hirtzig, M., et al. (2006), Monitoring atmospheric phenomena on Titan, *Astron. Astrophys.*, *456*(2), 761–774.

Hourdin, F., O. Talagrand, R. Sadourny, R. Courtin, D. Gautier, and C. P. McKay (1995), Numerical-simulation of the general-circulation of the atmosphere of Titan, *Icarus*, *117*(2), 358–374.

Hueso, R., and A. Sànchez-Lavega (2006), Methane storms on Saturn's moon Titan, *Nature*, *442*(7101), 428–431.

James, I. N. (1994), *Introduction to Circulating Atmospheres*, Cambridge Univ. Press, New York.

Lindal, G. F., G. E. Wood, H. B. Hotz, D. N. Sweetnam, V. R. Eshleman, and G. L. Tyler (1983), The atmosphere of Titan—An analysis of the voyager-1 radio occultation measurements, *Icarus*, *53*(2), 348–363.

Lopes, R. M. C., et al. (2007), Cryovolcanic features on Titan's surface as revealed by the Cassini Titan Radar Mapper, *Icarus*, *186*(2), 395–412.

Lorenz, R. D. (2000), Planetary science—The weather on Titan, *Science*, *290*(5491), 467–468.

Lorenz, R. D., C. P. McKay, and J. I. Lunine (1999), Analytic investigation of climate stability on Titan: Sensitivity to volatile inventory, *Planet. Space Sci.*, *47*(12), 1503–1515.

Lorenz, R. D., J. C. Zarnecki, M. C. Towner, M. R. Leese, A. J. Ball, B. Hathi, A. Hagermann, and N. A. L. Ghafoor (2007), Descent motions of the Huygens probe as measured by the surface science package (ssp): Turbulent evidence for a cloud layer, *Planet. Space Sci.*, *55*(13), 1936–1948.

Lorenz, R. D., et al. (2006), The sand seas of Titan: Cassini radar observations of longitudinal dunes, *Science*, *312*(5774), 724–727.

Mäkinen, J. T. T., A. M. Harri, T. Tokano, H. Savijärvi, T. Siili, and F. Ferri (2006), Vertical atmospheric flow on Titan as measured by the HASI instrument on board the Huygens probe, *Geophys. Res. Lett.*, *33*, L21803, doi:10.1029/2006GL026982.

McKay, C. P., J. B. Pollack, and R. Courtin (1989), The thermal structure of Titan's atmosphere, *Icarus*, *80*(1), 23–53.

McKay, C. P., J. B. Pollack, and R. Courtin (1991), The greenhouse and antigreenhouse effect on Titan, *Science*, *253*(5024), 1118–1121.

Mitchell, J. L., R. T. Pierrehumbert, D. M. W. Frierson, and R. Caballero (2006), The dynamics behind Titan's methane clouds, *Proc. Natl. Acad. Sci. U.S.A.*, *103*(49), 18,421–18,426.

Mitri, G., A. P. Showman, J. I. Lunine, and R. D. Lorenz (2007), Hydrocarbon lakes on Titan, *Icarus*, *186*(2), 385–394.

Niemann, H. B., et al. (2005), The abundances of constituents of Titan's atmosphere from the GCMS instrument on the Huygens probe, *Nature*, *438*(7069), 779–784.

Pierrehumbert, R. T. (2005), Climate dynamics of a hard snowball earth, *J. Geophys. Res.*, *110*, D01111, doi:10.1029/2004JD005162.

Porco, C. C., et al. (2005), Imaging of Titan from the Cassini spacecraft, *Nature*, *434*, 159–168, doi:10.1038/nature03436.

Rannou, P., F. Montmessin, F. Hourdin, and S. Lebonnois (2006), The latitudinal distribution of clouds on Titan, *Science*, *311*(5758), 201–205.

Robock, A., K. Y. Vinnikov, C. A. Schlosser, N. A. Speranskaya, and Y. K. Xue (1995), Use of midlatitude soil-moisture and meteorological observations to validate soil-moisture simulations with biosphere and bucket models, *J. Clim.*, *8*(1), 15–35.

Roe, H. G., I. de Pater, B. A. Macintosh, and C. P. McKay (2002), Titan's Clouds from Gemini and Keck Adaptive Optics Imaging, *Astrophys. J.*, *581*, 1399–1406, doi:10.1086/344403.

Roe, H. G., A. H. Bouchez, C. A. Trujillo, E. L. Schaller, and M. E. Brown (2005a), Discovery of temperate latitude clouds on Titan, *Astrophys. J.*, *618*, L49–L52, doi:10.1086/427499.

Roe, H. G., M. E. Brown, E. L. Schaller, A. H. Bouchez, and C. A. Trujillo (2005b), Geographic control of Titan's mid-latitude clouds, *Science*, *310*, 477–479, doi:10.1126/science.1116760.

Schaller, E. L., M. E. Brown, H. G. Roe, and A. H. Bouchez (2006), A large cloud outburst at Titan's south pole, *Icarus*, *182*, 224–229, doi:10.1016/j.icarus.2005.12.021.

Stofan, E. R., et al. (2006), Mapping of Titan: Results from the first Titan radar passes, *Icarus*, *185*(2), 443–456.

Stofan, E. R., et al. (2007), The lakes of Titan, *Nature*, *445*(7123), 61–64.

Thompson, W. R., J. A. Zollweg, and D. H. Gabis (1992), Vapor-liquid-equilibrium thermodynamics of n^2 + ch^4: Model and Titan applications, *Icarus*, *97*(2), 187–199.

Tobie, G., J. I. Lunine, and C. Sotin (2006), Episodic outgassing as the origin of atmospheric methane on Titan, *Nature*, *440*(7080), 61–64.

Tokano, T. (2005), Meteorological assessment of the surface temperatures on Titan: Constraints on the surface type, *Icarus*, *173*(1), 222–242.

Tokano, T., F. M. Neubauer, M. Laube, and C. P. McKay (2001), Three-dimensional modeling of the tropospheric methane cycle on Titan, *Icarus*, *153*(1), 130–147.

Tokano, T., F. Ferri, G. Colombatti, T. Mäkinen, and M. Fulchignoni (2006a), Titan's planetary boundary layer structure at the Huygens landing site, *J. Geophys. Res.*, *111*, E08007, doi:10.1029/2006JE002704.

Tokano, T., C. P. Mckay, F. M. Neubauer, S. K. Atreya, F. Ferri, M. Fulchignoni, and H. B. Niemann (2006b), Methane drizzle on Titan, *Nature*, *442*(7101), 432–435.

West, R. A., M. E. Brown, S. V. Salinas, A. H. Bouchez, and H. G. Roe (2005), No oceans on Titan from the absence of a near-infrared specular reflection, *Nature*, *436*(7051), 670–672.

Zarnecki, J. C., et al. (2005), A soft solid surface on Titan as revealed by the Huygens surface science package, *Nature*, *438*(7069), 792–795.

J. L. Mitchell, School of Natural Sciences, Institute for Advanced Study, Einstein Drive, Princeton, NJ 08540, USA. (mitch@ias.edu)